Effects of Terrain Heights and Sizes on Island-Scale Circulations and Rainfall for the Island of Hawaii during HaRP

YANG YANG AND YI-LENG CHEN

Department of Meteorology, SOEST, University of Hawaii at Manoa, Honolulu, Hawaii

(Manuscript received 9 August 2006, in final form 23 April 2007)

ABSTRACT

Islands in Hawaii have different sizes and terrain heights with notable differences in climate and weather. In this study, the fifth-generation Pennsylvania State University–NCAR Mesoscale Model (MM5) land surface model (LSM) is used to conduct numerical simulations for the island of Hawaii with different model terrain heights and sizes during the diurnal cycle for the Hawaiian Rainband Project (HaRP) period. In addition to island blocking and orographic lifting, terrain heights also affect the land surface thermal forcing throughout the diurnal cycle by the variations of orographic clouds during the day and by the variations of the longwave radiation heat loss at night. The simulated rainfall distributions and amounts throughout the diurnal cycle are closely related to rising motions caused by nonlinear interactions among island blocking, orographic lifting, and land surface processes. Besides the terrain/mountain height, island size is another factor that affects rainfall production and distribution in Hawaii, because island size affects orographic lifting, surface forcing, and the advection time scale for an air parcel to reach the mountaintop. The heavy rainfall maximum on the mountaintop of the island of Kauai is due to its suitable height and size. This study confirms that the evening rainfall maximum along the western Kona leeside coast is caused by the convergence between the westerly return flow and the offshore flow. For a lower model terrain, the westerly return flow is weaker; as a result, there are smaller evening rainfall amounts.

1. Introduction

In the Hawaiian Island chain, islands have different sizes and terrain heights with notable differences in climate and weather. The island of Hawaii is the southeasternmost and the largest island in the Hawaiian island chain, with a diameter of roughly 140 km. Its topography is dominated by two volcanic mountains: Mauna Loa and Mauna Kea (>4100-m elevation) with Hilo on its eastern windward side (Fig. 1a). The upstream easterly trade wind flow is characterized by a moist conditionally unstable layer (2 km) with a low CAPE (<100 J kg^{-1}) (Carbone et al. 1998).

Effects of terrain heights on mountain-induced circulations have been studied extensively with idealized numerical studies (e.g., Smolarkiewicz and Rotunno 1989, 1990; Schär and Durran 1997). For a stably stratified airflow past a bell-shaped axisymmetric mountain without considering diabatic heating, surface friction, and the diurnal heating cycle, either the Froude number (Fr = U/Nh, where U is the upstream wind speed, N is the Brunt–Väisälä frequency, and h is the height of the barrier) or the nondimensional mountain height (H_m = 1/Fr) is a control parameter for the flow regime. For the flow of a single layer of shallow water past a 3D isolated topography, Schär and Smith (1993) show the dependence of flow on the ratio of mountain height to fluid depth ($M = h/H$), where H is the depth of the lower fluid. However, the land surface forcing (surface thermal forcing and friction) was ignored in these studies and was crudely treated in previous numerical studies of the island-scale circulations on the island of Hawaii (Nickerson 1979; Smolarkiewicz et al. 1988; Rasmussen et al. 1989; Ueyoshi and Han 1991; Rasmussen and Smolarkiewicz 1993; Feng and Chen 2001).

Observational studies of island-scale airflow and weather for the island of Hawaii (e.g., Leopold 1949; Eber 1957; Lavoie 1967; Mendonca 1969; Garrett 1980; Chen and Nash 1994; Chen and Wang 1994, 1995; Feng and Chen 1998; Frye and Chen 2001; Carbone et al. 1995) showed the significant effects of land surface thermal forcing on the island-scale weather and climate

Corresponding author address: Prof. Yi-Leng Chen, Dept. of Meteorology, University of Hawaii at Manoa, Honolulu, HI 96822. E-mail: yileng@hawaii.edu

DOI: 10.1175/2007MWR1984.1

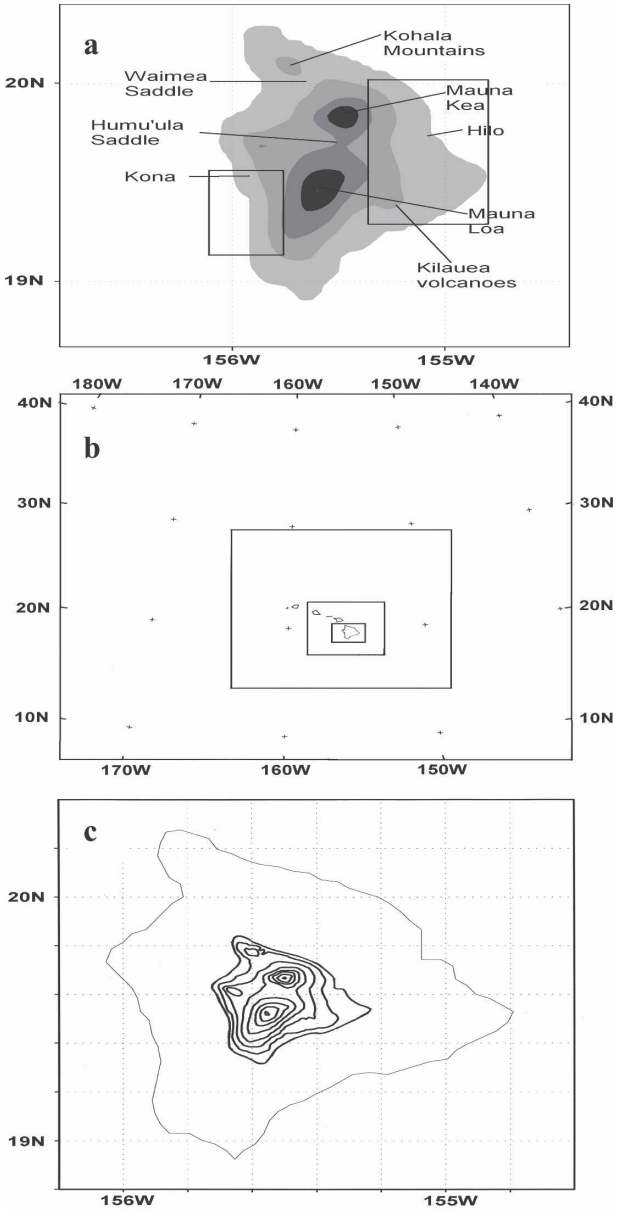

FIG. 1. (a) Map of the island of Hawaii with terrain height shown by gray shading, scale of 1000 m from light to dark (the same hereafter). (b) The four domains employed in this study have resolutions of 81, 27, 9, and 3 km, respectively. (c) The shrunken terrain of the island of Hawaii from TER35 with a contour interval of 200 m (thick solid lines). The thin solid line is the real coastline of the island of Hawaii. The two quadrangles in (a) are used for statistic analysis in section 4.

in Hawaii. Chen and Nash (1994) showed that in regions of weak mean surface winds caused by island blocking, the thermally driven diurnal winds become significant. In the Kona area on the western lee side where easterly trades are absent, the diurnal variations of local winds are mainly driven by the land–sea thermal contrast with the longest duration of anabatic/upslope flow along the Kona leeside coastline (Yang and Chen 2003; Chen and Nash 1994). Furthermore, in addition to feedback effects of latent heat release (Chen and Feng 2001), the variations of orographic cloud cover and the amount of water vapor in the atmosphere due to different terrain/mountain heights could affect the thermal forcing from the surface and feed back to the island-scale airflow and weather. Therefore, without careful consideration of the land surface thermal forcing in the model, our understanding of the effects of terrain/mountain heights on the island-scale circulations and weather in Hawaii is incomplete.

In Hawaii, island size may be another factor that can affect the island-scale circulations, weather, and climate. Terrain size is used as a factor to determine the surface friction (Grubišić et al. 1995) and surface thermal forcing (Reisner and Smolarkiewicz 1994), which can affect the island-scale circulations. From a linear theory of moist stable orographic precipitation, Smith and Barstad (2004) suggested that the location of the rainfall maximum shifts from the windward slope to the hilltop as mountain width decreases. For narrow mountains and high wind speeds, spillover is possible.

Rainfall analyses in Hawaii showed the dependence of the rainfall maximum location on mountain heights (Giambelluca et al. 1986). For mountains with peaks above the trade wind inversion (~2 km), maximum rainfall occurs on the windward slopes. For islands with mountaintops below the trade wind inversion, maximum rainfall occurs on the mountaintops. The island of Kauai, the northernmost island in Hawaii, with a maximum mountain elevation of 1500 m and a diameter of 50 km, is known as one of the wettest places in the world with the rainfall maximum (12 000 mm yr^{-1}) on its mountaintop (Ramage and Schroeder 1999). It is commonly believed that the mountain height controls whether the maximum rainfall occurs over the wind slopes or the crest of the mountain (Giambelluca et al. 1986). However, island/terrain sizes are ignored for the rainfall production and distribution over the Hawaiian Islands.

The overall objective of this study is to investigate the effects of terrain/mountain height and size on island-scale circulations and rainfall production for the island of Hawaii with a thorough consideration of the land surface forcing (surface thermal forcing and friction). We use the fifth-generation Pennsylvania State University–National Center for Atmospheric Research (PSU–NCAR) Mesoscale Model (MM5) to conduct sensitivity tests with different model terrain heights and

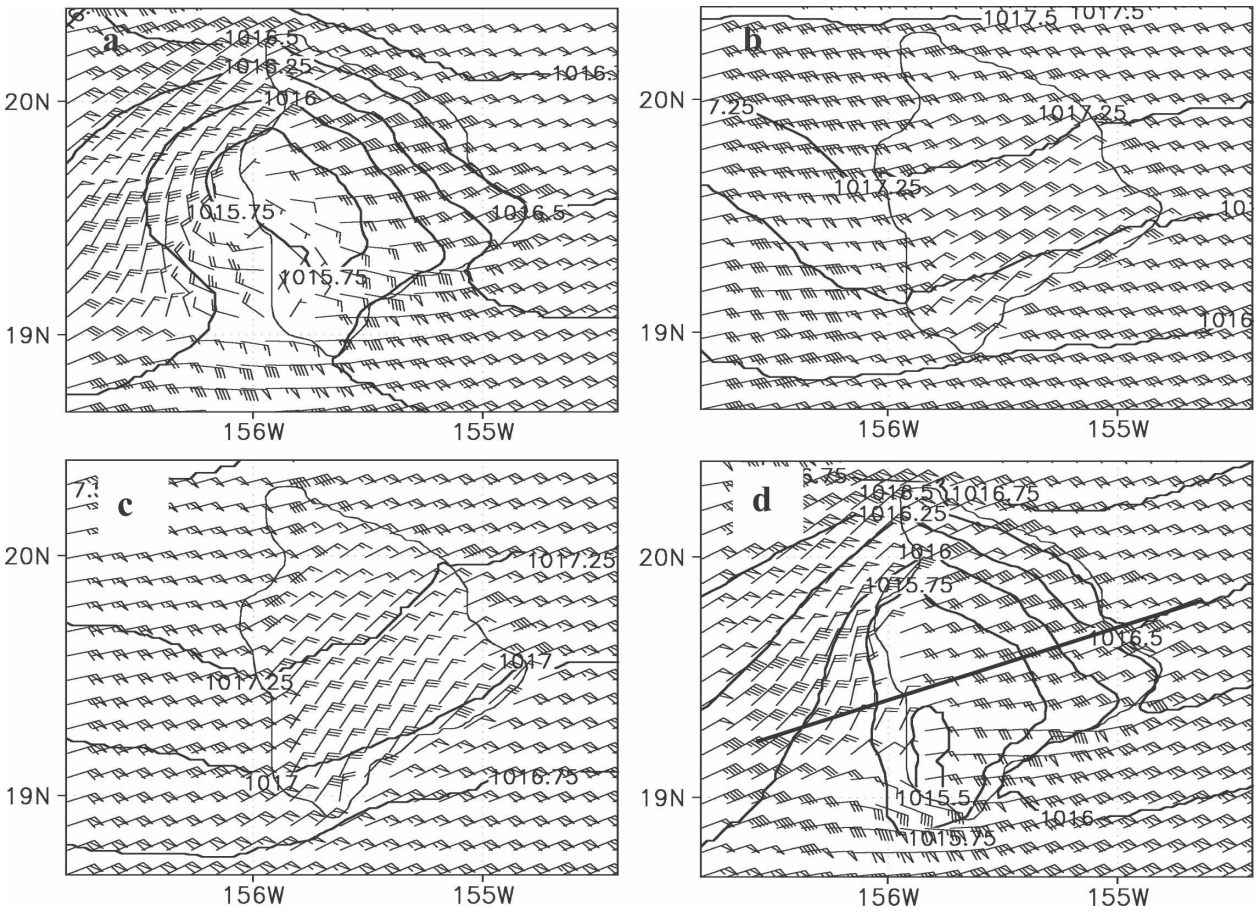

FIG. 2. Temporal mean surface winds and pressure with an interval of 0.25 hPa for TER00 during the HaRP period at (a) 1700, (b) 2100, (c) 0500, and (d) 1300 HST. The thick solid line is the transect for vertical cross sections. Pennants, full barbs, and half barbs represent 5, 1, and 0.5 m s^{-1}, respectively (the same hereafter)

sizes for the island of Hawaii, because the island-scale circulations of the island of Hawaii during the diurnal cycle are well simulated by the model with proper treatment of the lower boundary conditions (Yang et al. 2005).

Carbone et al. (1998) showed that the rainfall on the windward side of the island of Hawaii increases for a higher Fr with a greater wind speed as a result of island blocking. The correlation between rainfall and Fr could be interpreted by stronger orographic lifting as the wind speed increases. A higher Fr could be achieved by lowering the mountain height without changing the wind speed. We will test if Fr is a control parameter for the rainfall production on the windward side or not.

On the lee side of the island of Hawaii, maximum rainfall occurs in the Kona area. Leopold (1949) suggested that the rainfall there is caused by the clouds that form over land or near the shore and drift inland with the sea breezes. Giambelluca et al. (1986) suggested that the convergence between the trade wind flow through the saddle and the sea breezes is the main reason. Patzert (1969) speculated that the maximum rainfall is probably due to the convergence zone between the two counterrotating vortices in the lee. Yang and Chen (2003) found that in the Kona coastal region, the diurnal rainfall maximum occurs in the evening, most likely caused by the convergence between the dynamically induced westerly return flow in the wake (Patzert 1969; Smith and Grubišić 1993) and the land breezes. In this study, we will study the role of orographic lifting on the rainfall production on the Kona slopes in the afternoon, and the effects of terrain heights on the leeside circulations and rainfall.

2. Model description and initialization

The MM5 (Dudhia 1993) is a nonhydrostatic, three-dimensional primitive equation model employing the terrain-following sigma vertical coordinate. In this

study, there are 36 sigma levels[1] from the surface to the 100-hPa level. Four nested domains with two-way nesting were used with horizontal resolutions of 81, 27, 9, and 3 km (Fig. 1b). A Grell cumulus parameterization, grid-scale warm rain process (Hsie et al. 1984), a cloud-radiation scheme (Dudhia and Moncrieff 1989), and Hong and Pan's (1996) boundary layer scheme are used in the model. The land surface model (LSM) has four layers at depths of 10, 40, 100, and 200 cm (Chen and Dudhia 2001).

To study the effects of island blocking and orographic lifting on the rainfall production, we use the MM5 LSM as a research tool. Besides the control simulation with the real terrain of the island of Hawaii (referred to as CTRL) (Yang et al. 2005), we conducted simulations with terrain heights of 70% (referred to as TER70) and 35% (referred to as TER35) of the real terrain. In addition, a flat island with 0.1-m elevation (referred to as TER00) of the island of Hawaii is conducted to study the effects of land surface forcing on island-scale airflow and rainfall without island blocking. To determine if the island size is important for the observed large trade wind rainfall at the mountaintop of the island of Kauai, we conducted another simulation with a shrunken terrain of about 1/7 of the size of TER35 (referred to as S_TER), approximately the size and terrain height of the island of Kauai.

In the Hawaiian Islands, the occurrence of steep terrain, heterogeneous soil properties, and vegetation cover causes large spatial variations in local weather and climate, ranging from humid tropical conditions on the windward side to semiarid desert on the lee side. For our CTRL, the 1-km vegetation type, soil type, and vegetation fraction compiled by Zhang et al. (2005a,b) were used to improve the land surface properties for the LSM. The initial soil moistures and soil temperatures for LSM were generated from 2-month simulations before the start of the Hawaiian Rainband Project (HaRP; 11 July–24 August 1990).

The daily simulation for the HaRP period was initialized at 1200 UTC each day using the 24-h forecasts of the soil moistures and soil temperatures of the previous day and run for 36 h. The results from hours 12 to 36 for each simulation were used to represent the simulated diurnal cycle of the following day. The initialization of the MM5 LSM and the land surface properties (vegetation cover, soil type, and land use type) for

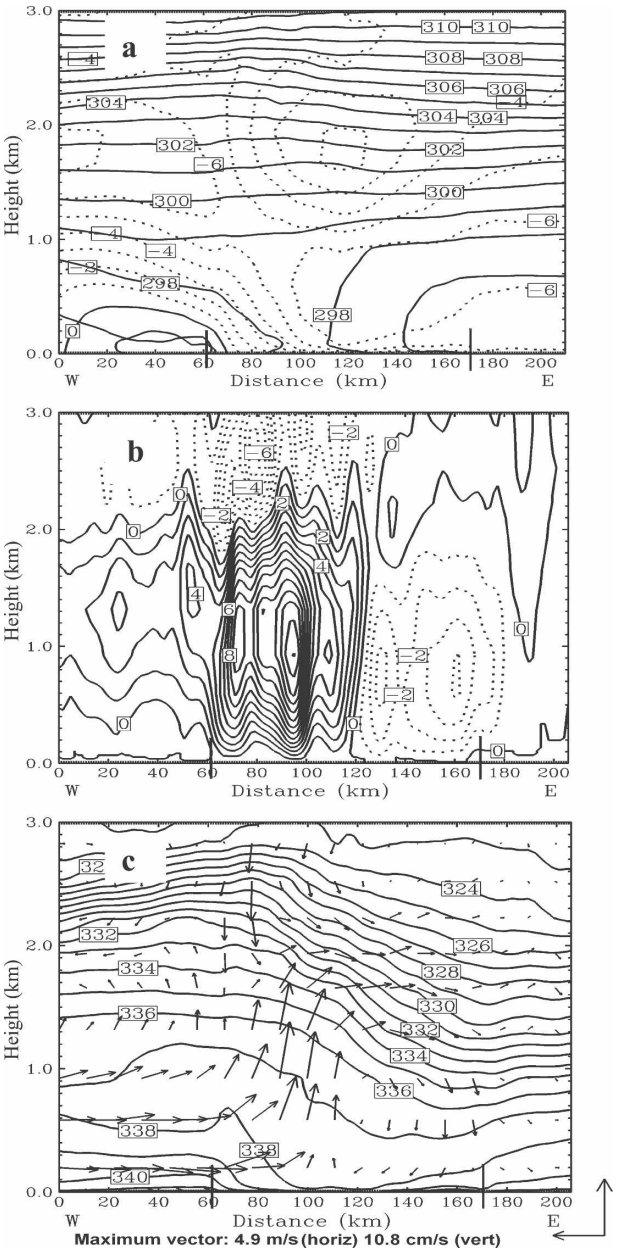

FIG. 3. Height–distance (km) cross sections along the transect in Fig. 2d at 1700 HST. (a) Mean zonal wind speed with a contour interval of 1 m s^{-1} and potential temperature (K) with a contour interval of 1 K during the HaRP period. (b) Mean vertical velocity with an interval of 1 cm s^{-1}. (c) Vectors of wind speed deviations from the daily mean and temporal mean equivalent potential temperature (K) with a contour interval of 1 K. Thick short straight lines across the x axes show roughly the coastlines.

TER70, TER35, and TER00 and the run procedures are the same as for CTRL, except that the initial ground temperature and soil temperatures for these sensitivity tests at 1200 UTC 10 July were adjusted from CTRL according to the terrain height with a lapse rate of 0.6 K (100 m)$^{-1}$. The vegetation type, soil type, and

[1] The full sigma levels are 1.000, 0.999, 0.998, 0.996, 0.994, 0.992, 0.990, 0.988, 0.985, 0.980, 0.97, 0.945, 0.91, 0.865, 0.82, 0.79, 0.76, 0.73, 0.7, 0.67, 0.64, 0.61, 0.58, 0.55, 0.52, 0.475, 0.425, 0.375, 0.325, 0.275, 0.225, 0.175, 0.125, 0.075, 0.025, and 0.000.

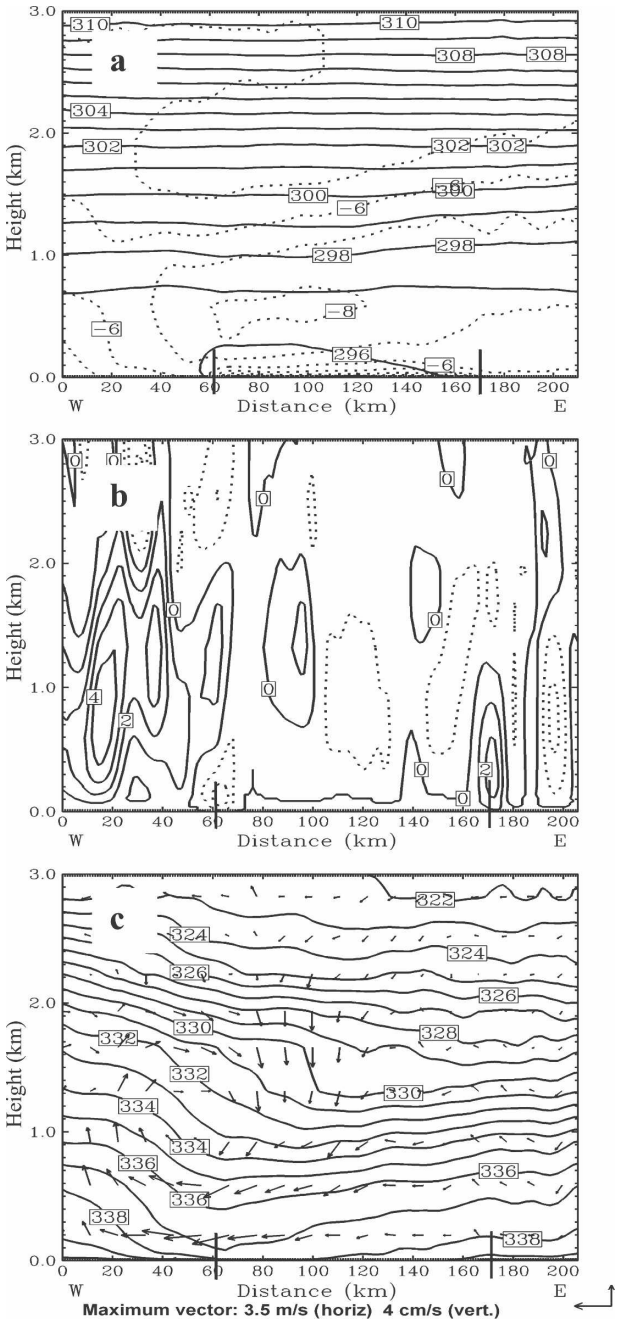

FIG. 4. Same as in Fig. 3 but at 2100 HST.

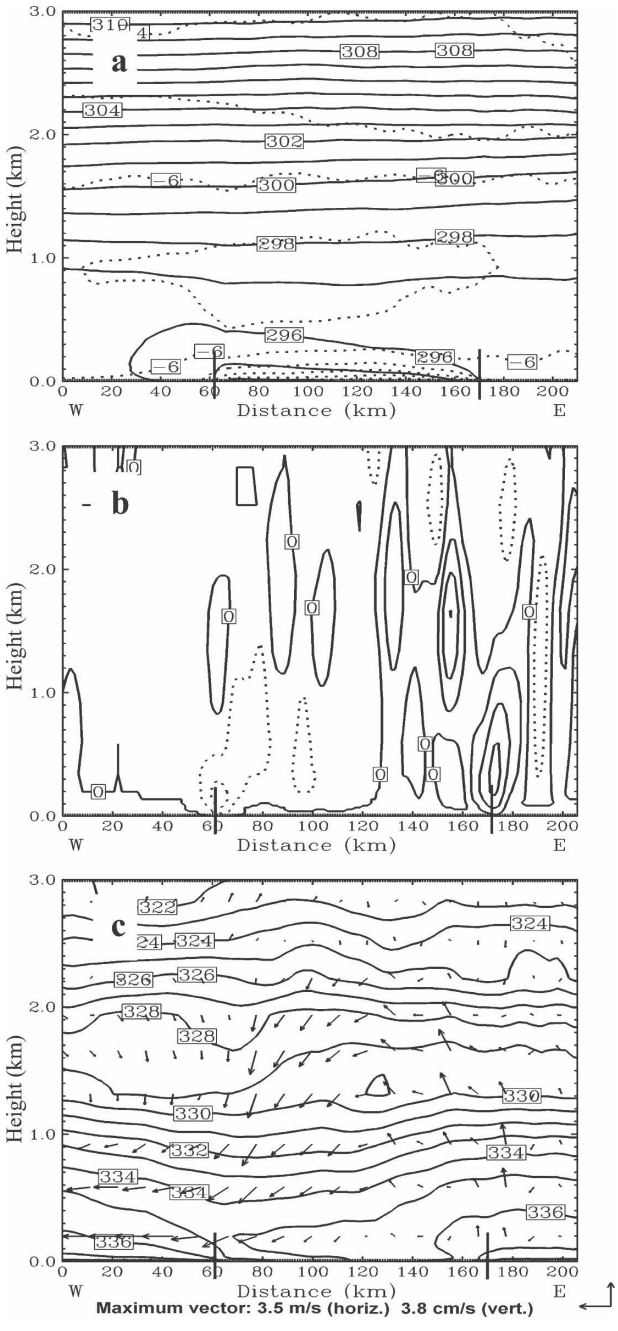

FIG. 5. Same as in Fig. 3 but at 0500 HST.

vegetation fraction for S_TER are shrunk from TER35 with the same procedures as the terrain so that the horizontal distribution of these surface parameters is similar to TER35. To resolve the shrunk terrain in S_TER better, the smallest domain in S_TER (Fig. 1c) has a horizontal resolution of 1.5 km. All of the simulations for the sensitivity tests are conducted for the HaRP period.

3. Island-scale circulations and weather without mountains

Chen and Nash (1994) suggest that the diurnal variations of rainfall and winds over the island of Hawaii are results of nonlinear interactions among land surface forcing, island blocking, and orographic lifting. In this section, to isolate the effects of land surface forcing on

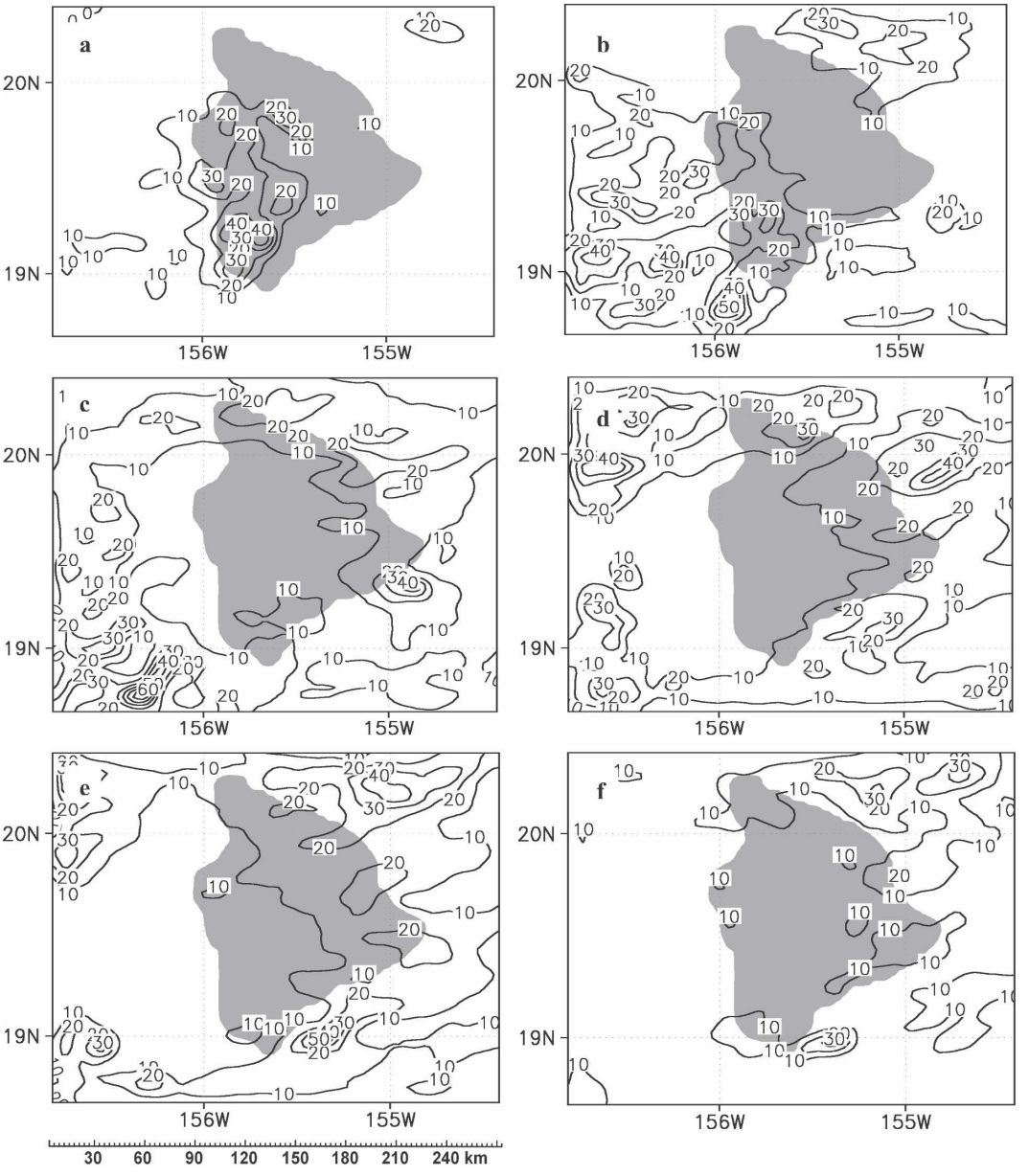

FIG. 6. Simulated 4-h rainfall accumulation for TER00 during the HaRP period with an interval of 10 mm for (a) 1500–1900, (b) 1900–2300, (c) 2300–0300, (d) 0300–0700, (e) 0700–1100, and (f) 1100–1500 HST. Shading shows the flat terrain of the island of Hawaii.

island-scale circulations and rainfall, we conduct simulations of the diurnal cycle without terrain for each HaRP day.

a. Diurnal surface winds and temperature

In the afternoon, land surface heating produces lower pressure over land than over the ocean (Figs. 2a and 2d). The land surface pressure minimum corresponds to a maximum temperature over the island interior (not shown) where the land surface is covered mainly by bare ground in the model. At night, land surface cooling results in pressure ridges over the island (Figs. 2b and 2c) with pressure contours oriented from northeast to southwest.

In the late afternoon (Fig. 2a), the surface trade wind speed on the windward side decreases from the ocean to the windward coast because of differential land–ocean surface friction. From the windward coast to the island interior, the surface winds are gradually strengthened down the surface pressure gradients (Fig. 2a). In

the area corresponding to the surface pressure minimum, the easterly surface wind speed decreases and meets the sea breezes over the leeside coastal region (Fig. 2a).

At night, the decrease of the surface wind speed from the ocean to the windward coastal region is more significant (Figs. 2b and 2c) than during the daytime (Figs. 2a and 2d), because of a higher pressure over land caused by nighttime cooling, in addition to differential land–ocean surface friction.

b. Vertical extents of local circulations

In the afternoon, rising motions occur on the leeside coastal region due to the convergence between the sea breezes and the opposing incoming airflow (Figs. 3a and 3b). The trade wind inversion is lifted slightly over the leeside coastal region by the rising motions (Fig. 3c). Sinking motion is noted on the windward side (Figs. 3b and 3c), which is perhaps related to the acceleration of the low-level winds toward the pressure minimum over the interior of the island.

Later in the evening, the cooling of the land causes a new pattern of circulations over the island (Figs. 4 and 5). At that point, rising motion develops over the windward coastal region (Fig. 4b) as the incoming flow decelerates (Fig. 4a). On the western lee side, the land-breeze front (or cold air) extends about 10 km offshore (Figs. 4a and 4c). The convergence between the land breezes and the slower trade wind flow downstream results in a rising motion off the leeside coast (Fig. 4b). At 0500 Hawaiian standard time (HST; Fig. 5a), with continued land surface cooling throughout the night, the rising motion on the windward side is deeper and stronger by 1 cm s^{-1} than in the evening (Figs. 4b and 5b). On the lee side, the land-breeze front (or cold air) extends 30 km farther offshore than in the evening (Figs. 4a and 5a). A sinking motion occurs over the leeside coastal region, where an acceleration of airflow leaving the island results from the pressure gradient force from the land to the ocean (Fig. 2c) and differential land–sea surface friction (Figs. 5b and 5c).

c. Simulated rainfall

Along the windward coastal region, rainfall occurs throughout the diurnal cycle, except in the afternoon (Fig. 6). The strongest rising motion on the windward side occurs in the early morning before dawn (Fig. 7c). As a result, the windward side has a nocturnal rainfall maxima (Fig. 6). It is apparent that the frequently observed early morning rainfall maximum along the windward coast of the Hawaiian Islands can be explained by land surface cooling and differential land–sea surface friction.

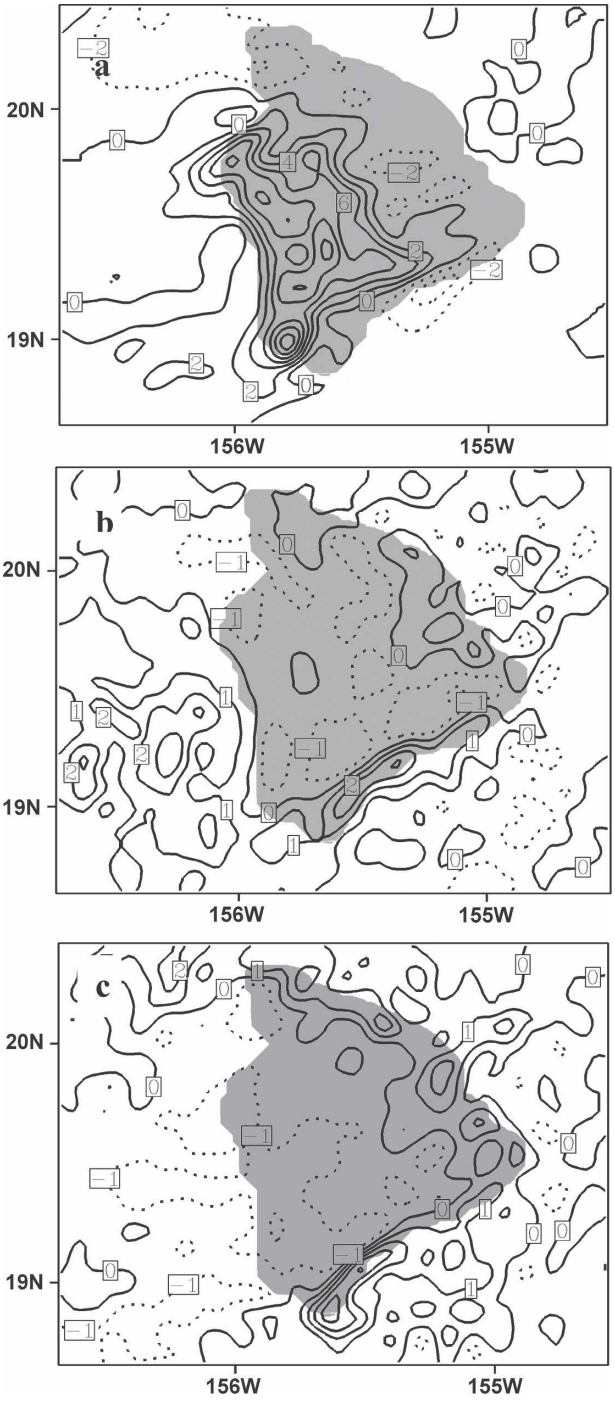

FIG. 7. Temporal mean vertical velocity at 500 m above the sea level during the HaRP period for TER00 at (a) 1700 HST with a 2 cm s^{-1} contour interval, and at (b) 2100 and (c) 0500 HST with a 1 cm s^{-1} interval. Shading shows the flat terrain of the island of Hawaii.

Along the leeside coastal region, rainfall mainly occurs in the late afternoon (Fig. 6a) and early evening

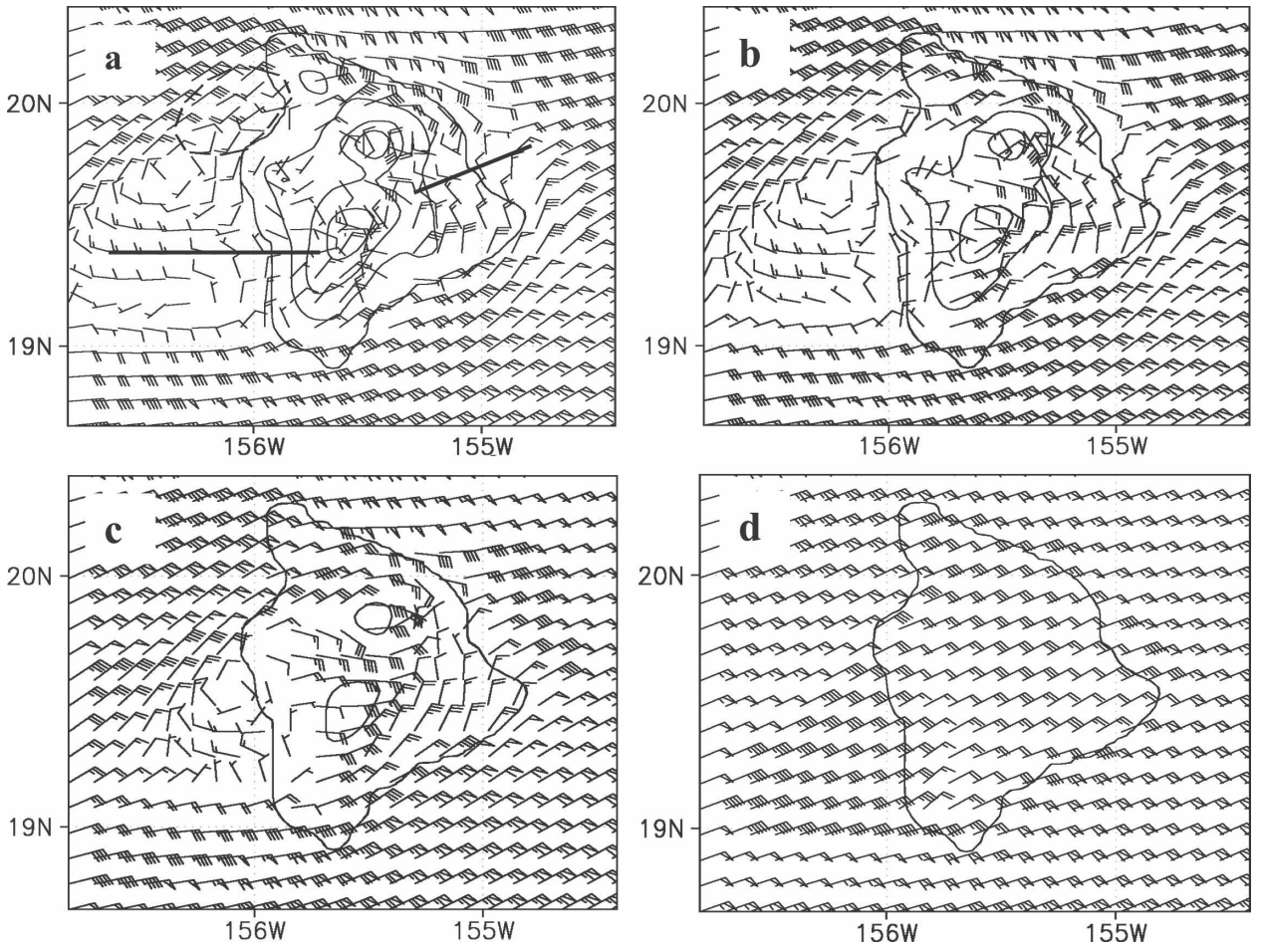

FIG. 8. Temporal mean surface winds during the HaRP period for (a) CTRL (the control run), (b) TER70, (c) TER35, and (d) TER00. Thin solid lines are terrain height contours with a 1000-m interval. Thick solid lines in (a) are transects for vertical cross sections and are referred to as the Kona transect for the western one and the Hilo transect for the eastern one in the text. Dashed lines in (a) show roughly the position of the small wake.

(Fig. 6b) corresponding to the rising motion during these times (Figs. 7a and 7b). A rainfall maximum also occurs over the ocean about 30 km off the leeside Kona coastline at night (Figs. 6b–d) as the accelerating land breeze converges with the slower trade wind flow downstream (Fig. 7b).

The simulated rainfall maximum along the windward coast during the HaRP period without mountains is 100 mm (not shown), which is much lower than the simulated rainfall maximum on the windward side (500 mm) in CTRL. For a model run with the real terrain of the island of Hawaii, but without surface sensible and latent heat flux during HaRP, the rainfall maximum on the windward side is lower than 200 mm (not shown). Neither dynamic forcing nor land surface forcing alone is adequate to account for the rainfall production on the windward side. The nonlinear interactions between land surface forcing and dynamical forcing are at work for the rainfall production on the windward side, and will be discussed further in the following sections.

4. Island forcing with different terrain heights

In this section, a comparison is made for the simulated island-induced airflow and rainfall among CTRL, TER70, and TER35 to understand the nonlinear interactions between the land surface forcing and island blocking.

a. Mean surface winds

On the windward side, the surface trade wind flow upstream of Hilo becomes weaker while approaching the island as a result of the island blocking. The mean surface trade wind flow upstream of Hilo is the strongest for TER00 (Fig. 8d) and the weakest for CTRL

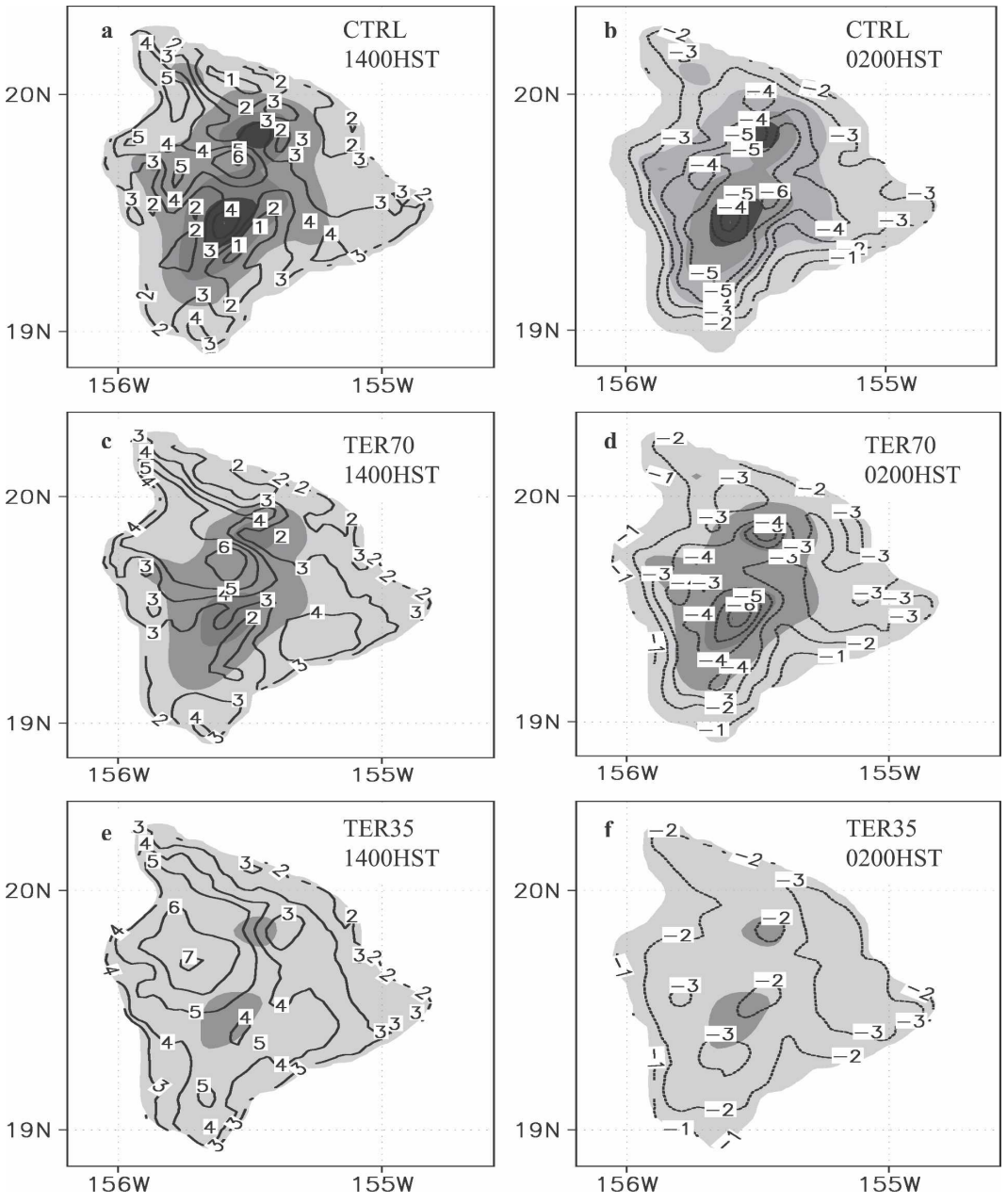

FIG. 9. The surface air temperature deviations from the mean upstream aircraft sounding during the HaRP period at the same level with a contour interval of 1 K for CTRL at (a) 1400 and (b) 0200 HST, for TER70 at (c) 1400 and (d) 0200 HST, and for TER35 at (e) 1400 and (f) 0200 HST.

(Fig. 8a). The flow deceleration becomes more significant with higher model terrain.

On the lee side of the Kohala Mountains, a small wake is simulated with a reversed flow of 2 m s^{-1} offshore for CTRL (Fig. 8a), consistent with observational studies (Smith and Grubišić 1993). For TER70 (Fig. 8b), the simulated small wake has a weak return flow. For TER35 (Fig. 8c), the small wake completely disappears. As the model terrain becomes lower, the flow over the northwestern area of the island shifts to a flow regime without a return flow in the lee. To the west of the Kona coast is the large wake zone (Smith and Grubišić 1993). Both CTRL and TER70 are in the same flow regime with the trade wind detouring around the island and the vortices in the lee. However, the horizontal extent of the large wake zone becomes smaller as the terrain height is reduced from CTRL to TER70. For TER35 with a flow regime of trade wind flow moving

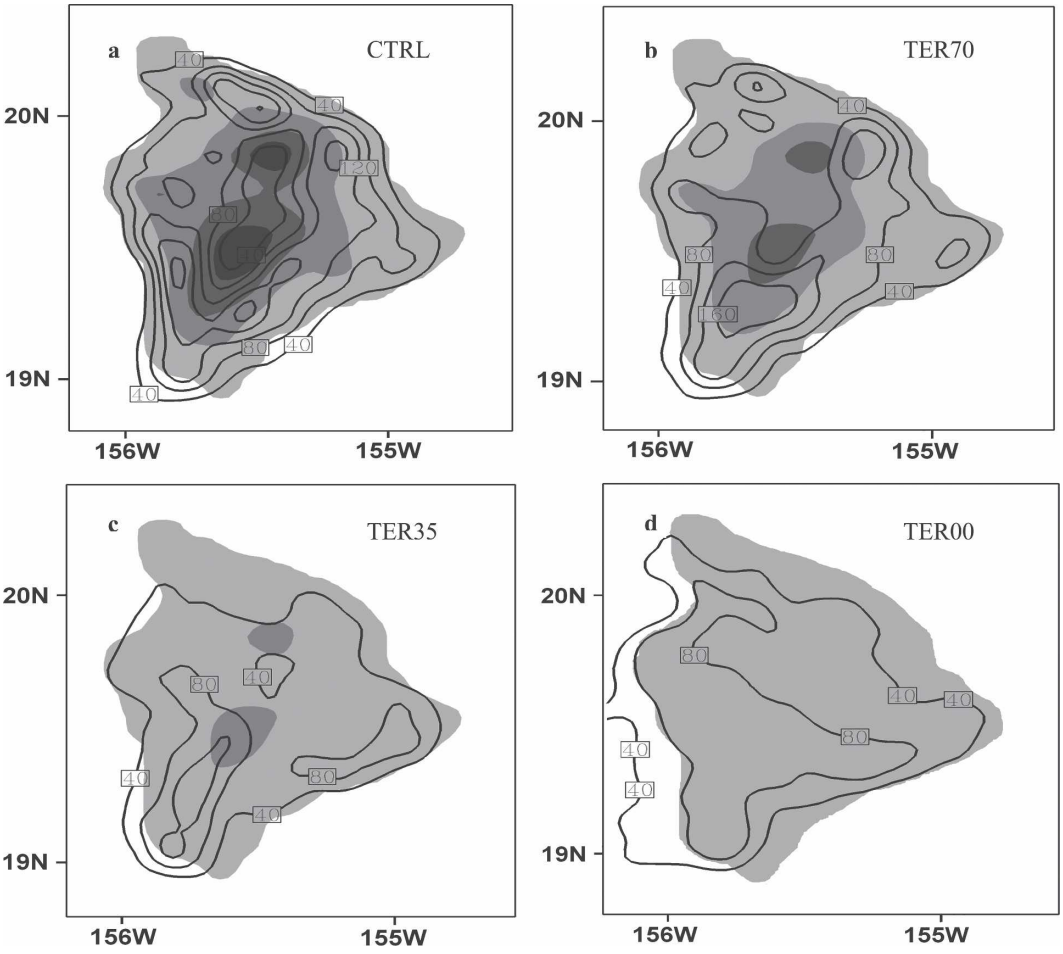

FIG. 10. Temporal mean of the vertical integrated mean cloud water content (10^{-3} mm) during the HaRP period at 1400 HST with a contour interval of 40 for (a) CTRL, (b) TER70, (c) TER35, and (d) TER00.

over the mountaintop, the leeside wake circulation is less significant than for CTRL and TER70.

b. Surface air temperature

During the daytime (Figs. 9a, 9c, and 9e), the positive surface air temperature deviations are greater on the leeside slopes than on the windward side, especially over the northwestern and southwestern leeside areas, the leeside areas of the Kilauea volcanoes, and the Humu'ula Saddle between Mauna Loa and Mauna Kea (Fig. 9). In the model, the land surface in these leeside areas is dominated by dry bare ground, whereas on the windward side, it is dominated by wet tropical forests. During the daytime, sensible heat fluxes are larger over dry bare ground than over wet tropical forests. Furthermore, adiabatic warming occurs on these leeside areas because of the significant descent of the trade wind flow aloft (Chen and Wang 1994; Yang and Chen 2003).

There are notable differences in surface temperature deviations among simulations with different mountain heights. For simulations with a lower mountain height, the surface air temperature deviations during the daytime are larger for most areas (Fig. 9). Note that except at the summits of Mauna Kea and Mauna Loa, the vertically integrated cloud water content is smaller for a lower model terrain (Fig. 10). With a lower model terrain, the orographic lifting is less significant with less cloudiness and higher insolation. In addition, on the leeside area of the Humu'ula Saddle, when the model terrain is lower, stronger adiabatic heating of the already warm air above the boundary layer top produces larger positive temperature perturbations.

At night, the simulated negative temperature deviations over land become smaller for simulations with lower model mountain heights, especially over the summits of Mauna Kea and Mauna Loa (5 K in CTRL; Fig. 9). The longwave radiation from the atmosphere to the

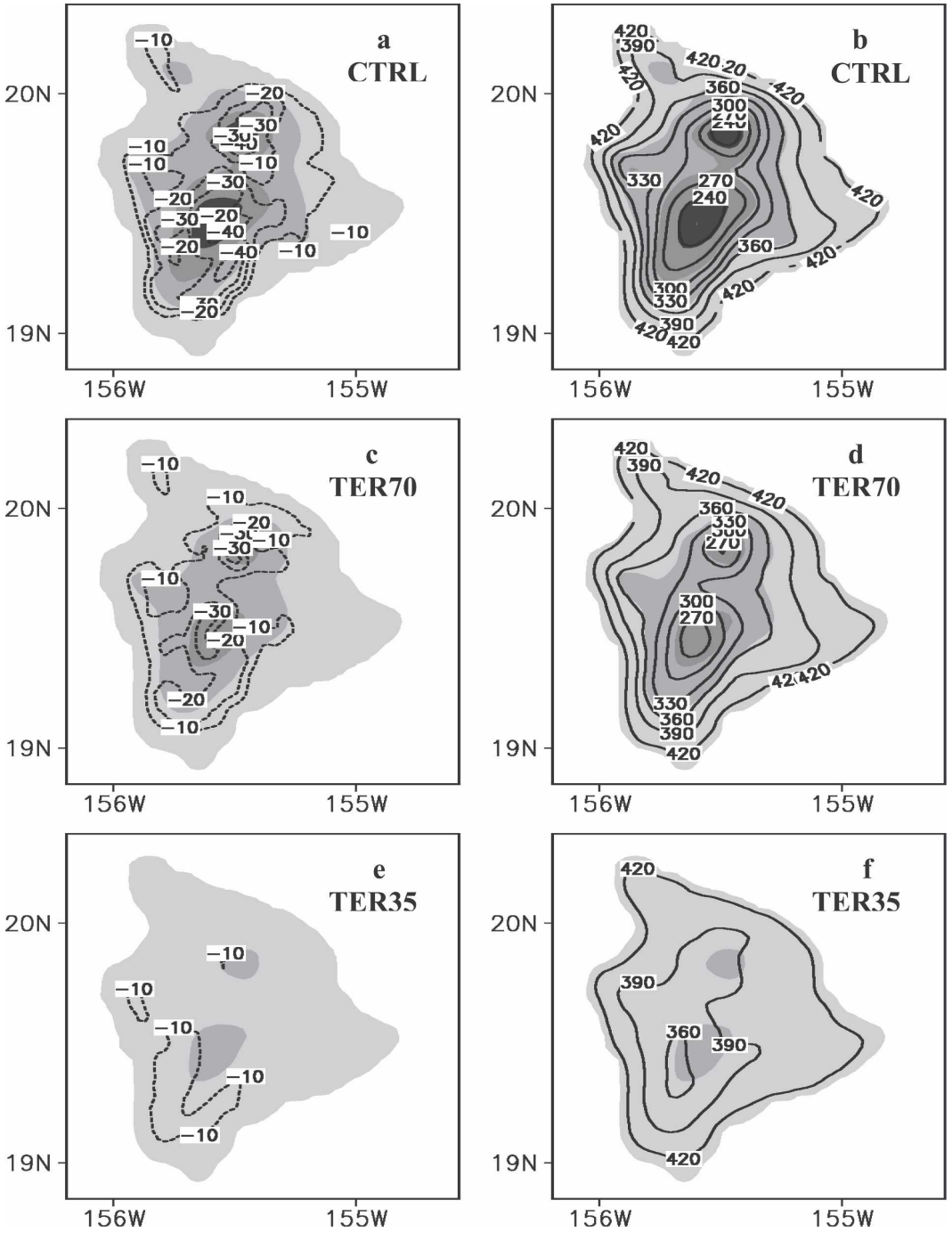

FIG. 11. Temporal mean surface sensible heating flux (W m^{-2}) for (a) CTRL, (c) TER70, and (e) TER35, and downward longwave radiation at the surface (W m^{-2}) for (b) CTRL, (d) TER70, and (f) TER35 at 0200 HST during the HaRP period.

ground depends on the amount of water vapor and air temperature in the atmosphere. As the summits are lower with more water vapor and warmer air above the surface, the downward longwave radiation is greater (Fig. 11). Note that from CTRL to TER70 and from TER70 to TER35, the downward longwave radiation at the surface on high-mountain areas increases by 30 and 70 W m^{-2}, respectively, whereas the negative sensible heating flux decreases by only 10 and 10–20 W m^{-2} (Fig. 11), respectively, indicative of less significant land

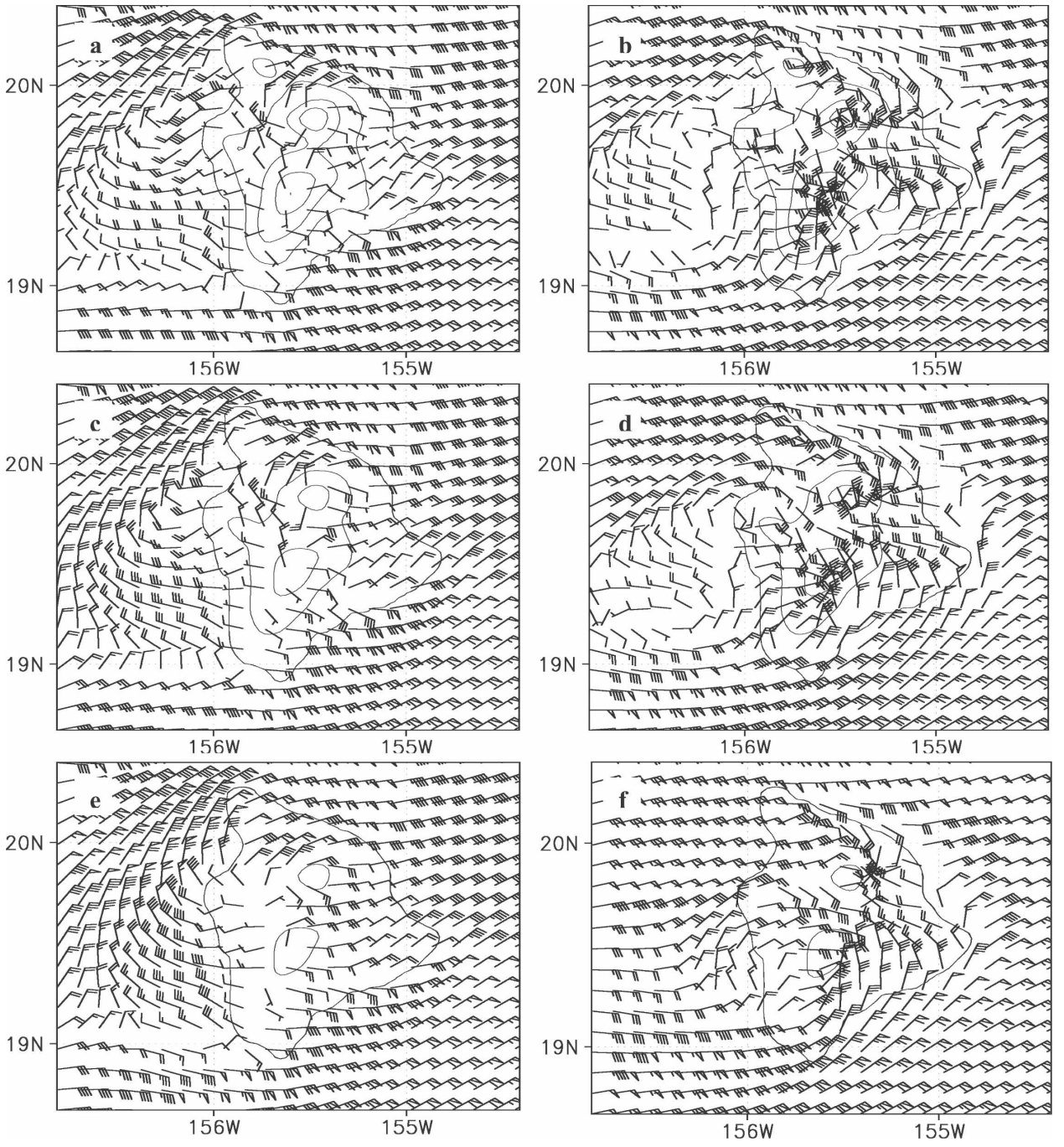

FIG. 12. Temporal mean surface winds during the HaRP period for CTRL at (a) 1400 and (b) 0200 HST, for TER70 at (c) 1400 and (d) 0200 HST, and for TER35 at (e) 1400 and (f) 0200 HST.

surface cooling at night as the model terrain becomes lower.

c. *Surface winds during the diurnal cycle*

For CTRL in the afternoon (Fig. 12a), upslope/onshore flow occurs over most of the windward and leeward areas. The westerly flow offshore off the Kona leeward coast has a wider north–south extent near the coastline than over the ocean. It merges with the sea breezes along the Kona coastal region and reaches a maximum strength in the afternoon hours. In the northwestern leeward areas, strong southwesterly winds (4

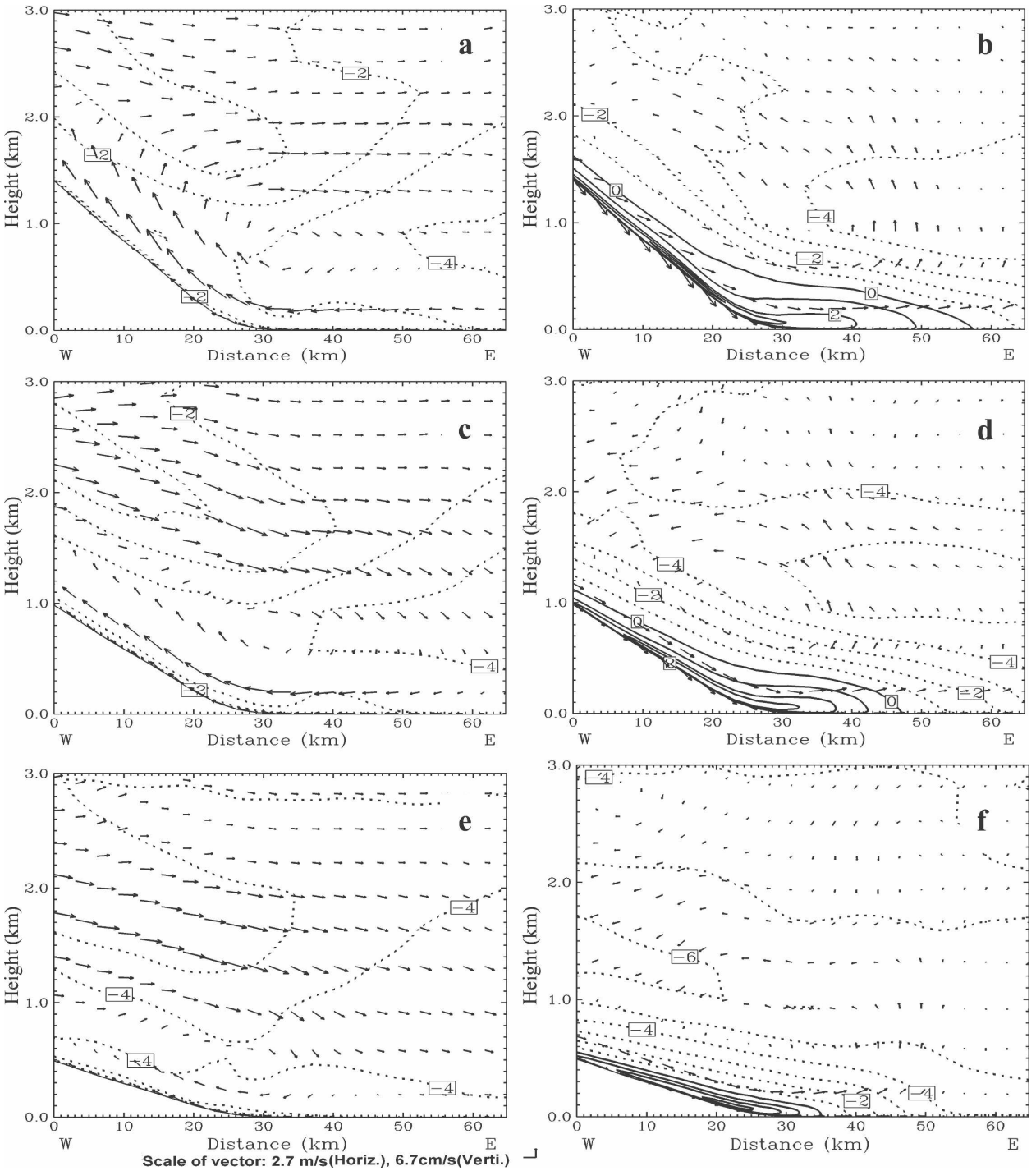

FIG. 13. Temporal mean zonal wind speed (m s^{-1}) with a contour interval of 1 m s^{-1} and vectors of wind speed deviations from the daily mean during the HaRP period for the Hilo transect (Fig. 8a) for CTRL at (a) 1400 and (b) 0200 HST, for TER70 at (c) 1400 and (d) 0200 HST (d), and for TER35 at (e) 1400 and (f) 0200 HST. Scale of vectors is shown at the bottom of (e).

m s^{-1}) occur in the afternoon as the dynamically induced return flow in the small wake (Smith and Grubišić 1993) merges with the sea breezes.

For TER35 and TER70, the onshore flow in the wake off the Kona coast during the daytime has a smaller horizontal extent than for CTRL (Figs. 12a, 12c, and 12e). The onshore flow in the small wake off the lee side of the Kohala Mountains fails to appear in

TABLE 1. Some characteristics of the temporal mean upslope flow on the windward side of the island of Hawaii at 1400 HST during the HaRP period, and the spatial mean of the rainfall accumulation (mm) for all of the grids in the quadrangle area (Fig. 1b) on the windward side for the time period 1100–1900 HST during HaRP.

	Fr	Max upslope flow ($m\ s^{-1}$)	Max rising motion ($cm\ s^{-1}$)	Rainfall (mm)
CTRL	0.2	2.5	16	67
TER70	0.3	3.5	13	28
TER35	0.6	4	8	20

TER35 (Fig. 12e). Along the leeside Kona coast, the afternoon sea breezes are stronger when the model terrain is lower because of stronger heating in the lee (Fig. 10).

At night (Fig. 12b), the simulated katabatic/offshore flow is simulated in CTRL over most of the windward side and leeward areas over land as in previous studies (Wang and Chen 1995; Feng and Chen 1998, 2001; Yang et al. 2005). The westerly return flow in the large wake zone encounters the offshore flow off the Kona coast. The north–south extent of the westerly return flow is narrower at night than in the afternoon. The dynamically induced return flow off the Kona coast is 0.5–1 $m\ s^{-1}$ weaker for TER70 than for CTRL (Figs. 12b and 12d). The return flow in the small wake is not simulated in the northwestern lee side for either TER70 or TER35. Off the Kona coast for TER35 (Fig. 12f), the horizontal extent of the westerly flow is smaller than for TER70 with a much weaker return flow offshore. The katabatic flow on the Kona slope on the lee side is slightly weaker for a lower model terrain height.

d. Vertical extents of local circulations on the windward side

Along the Hilo transect (Fig. 8a), the mean wind speeds of the combined trade wind–anabatic flows in the afternoon are 1–2.5, 2–3.5, and 3–4 $m\ s^{-1}$ for CTRL, TER70, and TER35, respectively (Figs. 13a, 13c, and 13e). For a lower model terrain, flow deceleration is less significant. Furthermore, with warmer surface air temperatures for a lower model terrain (Fig. 9), the anabatic flow is stronger. However, the orographic lifting is weaker for a lower model mountain height (Table 1; Fig. 14) because of a decrease in the mountain slope.

At 0200 HST, the maximum depths of the katabatic/offshore flow are 450, 400, and 200 m in the Hilo Bay area with offshore extents of 30, 20, and 5 km for CTRL, TER70, and TER35, respectively (Figs. 13b, 13d, and 13f, Table 2). The maximum katabatic/offshore flow is simulated over the lowlands with values of 4, 3.5, and 3 $m\ s^{-1}$ for CTRL, TER70, and TER35, respectively (Table 2). The katabatic/offshore flow on the windward side becomes shallower and weaker with a smaller offshore extent for a lower model terrain because of (i) a decrease in the steepness of the mountain slope, (ii) a stronger incoming trade wind flow offshore of Hilo (Fig. 8; Frye and Chen 2001), and (iii) smaller negative surface air temperature deviations. Lifting of the trade wind flow by the weaker and shallower katabatic/offshore flow becomes weaker and closer to the coast as the model terrain becomes lower (Fig. 14; Table 2). Orographic lifting near the coast is also weaker for a lower model terrain.

e. Vertical extents of local circulations on the leeward side

Along the Kona transect on the lee side (Fig. 8a), for CTRL at 1400 HST (Fig. 15a), the westerly flow extends 100 km offshore with a maximum wind speed of 3.2 $m\ s^{-1}$ at 400 m and its top at 1500 m. The upslope flow over the Kona slope has a maximum wind speed of 2 $m\ s^{-1}$ and a depth of 500 m (Table 3; Fig. 15a).

For TER70 (Fig. 15c), the westerly return flow off the Kona coast is shallower (1300 m) and extends only 90 km offshore. However, the onshore flow along the Kona coast and the upslope flow over the Kona slopes are stronger than CTRL, with maximum values of 3.8 and 2.5 $m\ s^{-1}$ (Table 3), respectively, because of larger surface air temperature deviations (Fig. 9). For TER35 (Fig. 15e), the vertical (1000 m) and horizontal (75 km) extents of the westerly flow are even smaller. However, the onshore flow along the Kona coast for TER35 is stronger (4.2 $m\ s^{-1}$) than for TER70 and CTRL with a stronger upslope flow on the Kona slope, because the surface air temperature deviations over land in the Kona area are the highest for TER35 (Fig. 9). However, the rising motions due to the orographic lifting on the leeside slopes are weaker for a lower model terrain (Table 3; Fig. 16).

At night, the simulated katabatic/offshore flow dominates the lowest levels in the Kona area in CTRL (Fig. 15b). The dynamically induced return flow with a maximum value of 2.5 $m\ s^{-1}$ (Table 4) is simulated in the wake. For TER70, the horizontal and vertical extents of the westerly flow offshore (Fig. 15d) are smaller than CTRL (Fig. 15b) because of weaker island blocking. For TER35 (Fig. 15f), the dynamically induced westerly return flow at night is limited to only the lowest levels (100 m) over the coastal areas with a relatively weak wind speed ($<0.5\ m\ s^{-1}$). The downslope flow over the Kona slope for TER35 is mainly the descending trade wind flow enhanced by land surface cooling. Rising motion occurs over the ocean near the Kona coast due to

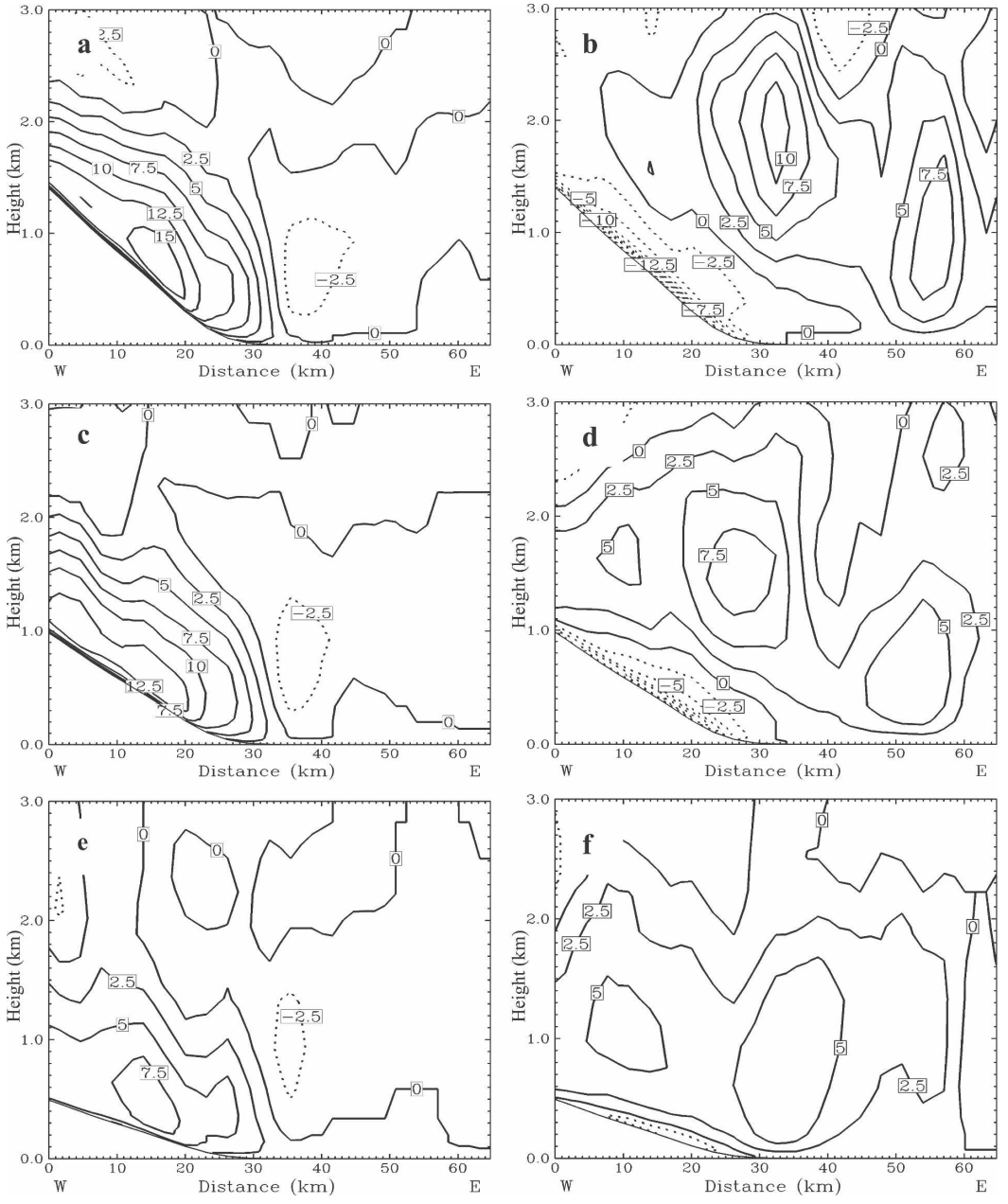

FIG. 14. Temporal mean vertical velocity (cm s^{-1}) with a contour interval of 2.5 cm s^{-1} during the HaRP period for the Hilo transect (Fig. 8a) for the control run at (a) 1400 and (b) 0200 HST, for TER70 at (c) 1400 and (d) 0200 HST (d), and for TER35 at (e) 1400 and (f) 0200 HST.

the convergence between the return flow and the offshore flow (Table 4; Fig. 16). The rising motion becomes weaker for a lower terrain.

f. Effect of terrain heights on rainfall

1) TOTAL RAINFALL

The total rainfall amount on the windward side is smaller and the rainfall maxima shift inland when model terrain height is lower (Fig. 17). For CTRL (Fig. 17a), the maximum rainfall axis is along the windward coast with a maximum of 500 mm to the southeast of Hilo. For TER70 (Fig. 17b), the maximum rainfall axis shifts inland to the lowland slopes with a maximum of 400 mm to the north of Hilo. For TER35 (Fig. 17c), the maximum rainfall axis shifts farther inland with a maximum of 300 mm to the northwest of Hilo. For TER00, the maximum rainfall on the windward

TABLE 2. Some characteristics of the temporal mean katabatic/offshore flow on the windward side of the island of Hawaii at 0200 HST during the HaRP period, and the spatial mean of the rainfall accumulation (mm) for all of the grids in the quadrangle area (Fig. 1b) on the windward side for the time period 1900–0300 HST during HaRP.

	CTRL	TER70	TER35
Fr	0.2	0.3	0.6
Max katabatic flow ($m\ s^{-1}$)	4	3.5	3
Max offshore extent (km)	28	18	5
Max depth (m)	450	400	200
Max rising motion on the leading edge ($cm\ s^{-1}$)	7.8	5.5	4.5
Max rising motion on the low slope ($cm\ s^{-1}$)	10.5	7.8	5.2
Rainfall accumulation (mm)	63	57	49

side is only 100 mm and it occurs along the coast (not shown).

For a lower model terrain, Fr is higher but the rainfall amount is smaller. This result is in contrast to the dependence of trade wind rainfall on Fr suggested by Carbone et al. (1998). Here, Fr is a control parameter for flow regimes but not a control parameter for rainfall production on the windward side. The rainfall amount is smaller if the terrain is lower or if the trade wind flow is weaker. It is apparent that orographic lifting is an important factor for the rainfall production on the windward side. However, orographic lifting alone may not be adequate to account for the observed trade wind rainfall (section 3c). Rainfall production during the diurnal cycle with different terrain heights will be discussed in the next section.

From a theoretical study of hydrostatic flow over an idealized mountain, Smith (1989) pointed out that "Kauai is about as high as it can be without flow splitting and therefore receives enormous rainfall" on mountaintops. For TER35, Fr has roughly the same value as that for Kauai. However, with a mountain height (1400 m) lower than the trade wind inversion in TER35, the rainfall maximum is not on mountaintops and it is lower than in CTRL (Fig. 17). It is interesting to note that islands with lower mountain heights within the Hawaiian Island chain are relatively small in size. Besides the mountain height, island size may also affect the rainfall distribution and production. This possibility will be further investigated in section 5.

2) DIURNAL VARIATIONS OF RAINFALL

Most of the simulated rainfall on the windward side during the diurnal cycle occurs at night (Figs. 18–20), which is consistent with observational studies (Chen and Nash 1994; Chen and Feng 1995). For CTRL, the maximum rainfall axis shifts from the lowland slope west of Hilo in the evening (Fig. 18b) to the ocean near the coast in the early morning (Fig. 18d) because of the development and gradual offshore extension of the katabatic/offshore flow (Chen and Nash 1994; Feng and Chen 2001). Chen and Nash (1994) suggest that the nocturnal rainfall production on the lower windward slopes is a result of low-level convergence between katabatic flow and the incoming decelerating trade wind flow and is enhanced by orographic lifting aloft. For a lower model terrain, the nocturnal rainfall maximum is lower because of weaker rising motions (Table 2). A smaller offshore extension of the katabatic/offshore flow for a lower model terrain (Table 2) results in shifting of the nocturnal rainfall maximum axis inland (Figs. 18–20).

In the afternoon hours, observational studies (Leopold 1949; Garrett 1980; Chen and Nash 1994) suggest that the trade wind rainfall on the windward slopes is caused by the orographic lifting of the combined trade wind–anabatic winds. For a lower model terrain, rainfall amounts during 1100–1900 HST (Figs. 18–20) on the windward slope are smaller because of weaker orographic lifting. For both 1900–0300 and 1100–1900 HST, the trade wind rainfall is positively correlated with maximum vertical motion and negatively correlated with Fr (Tables 1 and 2). However, the relationship between simulated vertical motions and the trade wind rainfall is not linear (Tables 1 and 2). In a conditionally unstable atmosphere, the vertical motion is not only forced by convergence and orographic lifting, it also depends on the feedback effects of the net condensation heating (Chen and Feng 2001).

On the western lee side of the island (Fig. 18), evening rainfall is mainly simulated along the Kona coastal region in CTRL. After midnight, rainfall mainly occurs over the ocean (Table 4) as the offshore flow extends farther offshore (Figs. 18c and 18d). For TER70, the dynamically induced return flow and circulation in the wake zone are weaker than in CTRL, resulting in a weaker rising motion (Table 4; Figs. 16b and 16d). The time-averaged low-level mixing ratio of water vapor off the central Kona coast over the HaRP period for TER70 is 0.5 $g\ kg^{-1}$ lower than for CTRL (not shown), perhaps as a result of weaker convergence between the westerly return flow and the offshore flow and less evaporation from the ocean surface by weaker winds in the wake zone for TER70 than for CTRL. All of these factors contribute to smaller rainfall amounts on the Kona coastal area for TER70 than for CTRL (Table 4). For TER35, besides a weaker wake circulation and convergence, the descending trade wind flow aloft moving over the low mountains (Fig. 16f) is an-

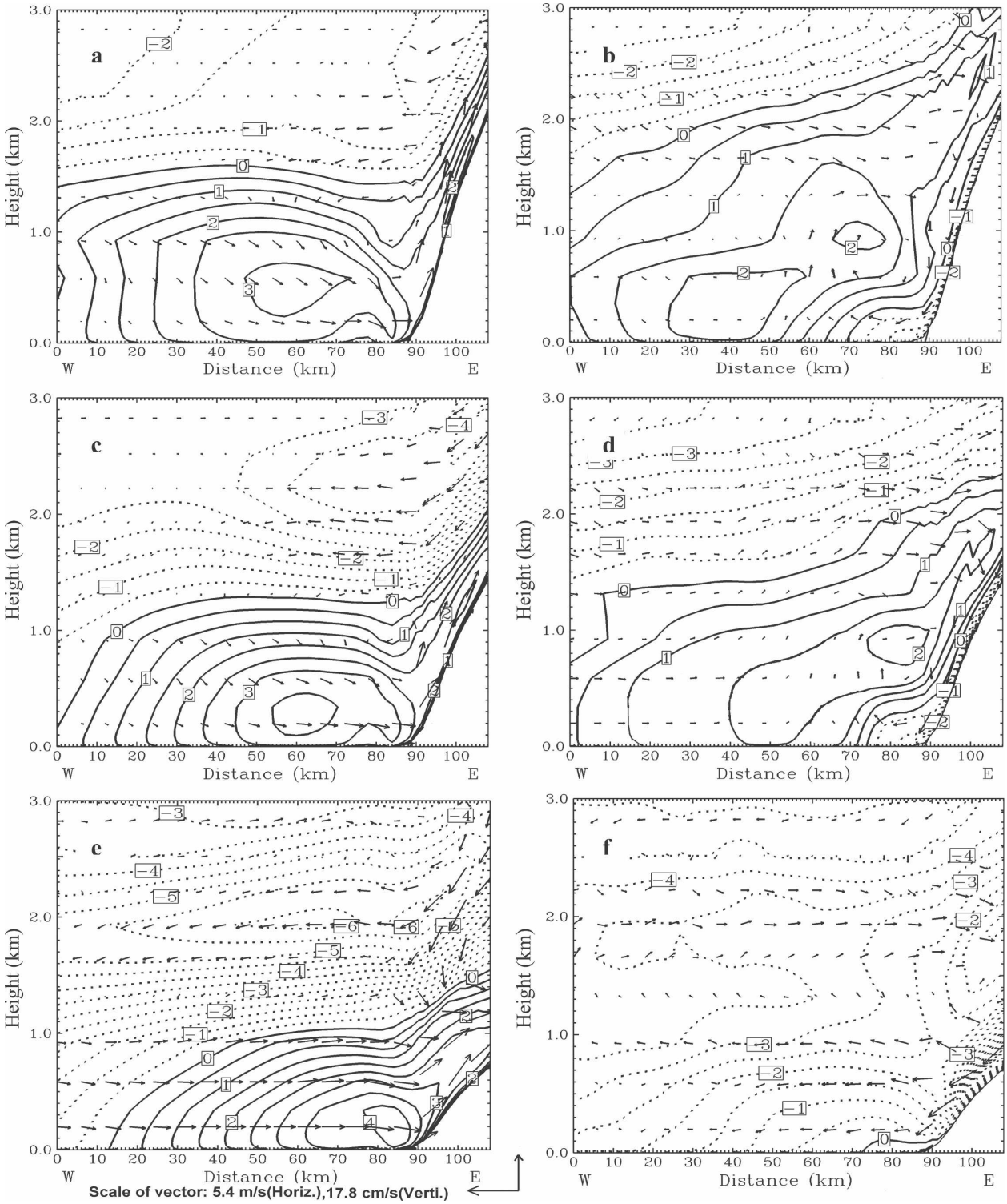

FIG. 15. As in Fig. 13 but for the Kona leeside transect.

other reason for less rainfall production on the lee side than for CTRL and TER70. The time-averaged mixing ratio over the Kona coastal region is 1–1.5 g kg^{-1} smaller than for TER70 and CTRL (not shown), perhaps due to the stronger descent of trade wind flow aloft and less evaporation from the ocean surface under weaker winds.

In the afternoon, rainfall on the leeside slopes is

TABLE 3. Some characteristics of the temporal mean upslope/onshore flow at 1400 HST during the HaRP period, and the spatial mean of the rainfall accumulation (mm) for all of the grids with an elevation of 200–2000 m in the quadrangle (Fig. 1b) on the lee side of the island of Hawaii for the time period 1100–1900 HST during HaRP.

	Fr	Max upslope flow ($m\ s^{-1}$)	Max onshore flow ($m\ s^{-1}$)	Max rising motion on the slope ($cm\ s^{-1}$)	Rainfall (mm)
CTRL	0.2	2	3.2	35	48
TER70	0.3	2.5	3.8	18	25
TER35	0.5	2.8	4.2	15	20

caused by rising motions due to the development of anabatic winds (Figs. 16a, 16c, and 16e). Weaker rising motions for a lower model terrain result in smaller rainfall amounts (Table 3). Similar to the windward side, rainfall amounts on the lee side are negatively correlated with Fr and positively correlated with vertical motions (Tables 3 and 4).

5. Circulations and rainfall with a reduced terrain area

In this section, we study the effects of island size on the island-scale circulations and rainfall distribution. With a smaller island size, the mountain slopes are steeper for the same mountain height. Furthermore, the land surface friction is less "viscous" for a smaller island size (Grubišić et al. 1995), because the bottom friction number in the shallow-water framework is proportional to the surface roughness, the horizontal scale of the obstacle, and the inverse of the upstream fluid depth. For S_TER with a terrain area about 1/7 of the CTRL, both the island height and size are comparable to those of Kauai.

a. Surface winds

With a much smaller island area in S_TER, the combined trade wind–upslope flow on the windward slopes in the afternoon (Fig. 21a) is 1–2 $m\ s^{-1}$ stronger than in TER35 (Fig. 12e). On the lee side of the island, the onshore/upslope flow is 1 $m\ s^{-1}$ weaker than in TER35. For S_TER, the surface air temperature perturbation is 1–3 K lower in the afternoon and 1–2 K higher during the nighttime than for TER35 (not shown). On the windward slopes, as will be shown later, the cloudiness for S_TER is greater with more rainfall production than for TER35. The heating rate in the afternoon and cooling rate at night on the windward slopes for S_TER would be smaller than for TER35. Furthermore, with a smaller island size and less upstream flow deceleration, it takes less time for the maritime air from the ocean to reach the island interior for S_TER than for TER35.

At night (Fig. 21b), the surface winds on the windward slopes are weaker with a more northerly direction than during the day (Fig. 21a). A very weak (0.5 $m\ s^{-1}$) and shallow (20 m deep) katabatic flow does not occur on the windward lowlands until the early morning (Figs. 21b and 22c). At 0200 HST, the katabatic flow on the windward low slopes in S_TER (Fig. 21b) is less pronounced than in TER35 (Fig. 12f).

b. Vertical extents of local circulations

During the daytime, orographic lifting results in rising motions on the windward slopes (Figs. 23a and 23d) with the maxima (40 $cm\ s^{-1}$) on the upper slopes, which is about 20–30 $m\ s^{-1}$ stronger than that on the windward side of TER35 (Fig. 14e). In the evening, the deceleration of the incoming trade wind flow on the windward side (Fig. 22b) by the surface friction is enhanced by the land surface cooling. The incoming trade wind flow near the surface on the windward side in the evening is weaker than the combined trade wind–anabatic flow in the afternoon (Figs. 22a and 22d). As a result, the orographic lifting on the windward side in the evening is 5–10 $cm\ s^{-1}$ weaker than in the late afternoon (Figs. 23a and 23b).

In the early morning, with continued land surface cooling, the deceleration of the incoming trade wind flow on the windward side is more significant than in the evening. On the windward slope, a zero contour line of zonal wind speed is discernable just above the slope surface (Fig. 22c). There is no corresponding sinking motion associated with the very weak and shallow katabatic flow (Fig. 23c). In contrast, for TER35, the katabatic flow on the slope has a maximum speed of 3 $m\ s^{-1}$ with a depth of 200 m (Fig. 13f; Table 2), because of cooler surface air temperatures and a weaker incoming flow for TER35 than S_TER. For S_TER, a maximum rising motion (15 $cm\ s^{-1}$) occurs on the lower windward slopes in the early morning due to the deceleration of the incoming trade wind flow (Fig. 23c) and orographic lifting aloft. The rising motion on the middle and upper slopes at this time is about 10–15 $cm\ s^{-1}$ weaker than in the afternoon (Figs. 23a, 23c, and 23d).

c. Rainfall

The simulated total rainfall maximum (600 mm) in S_TER near the Mauna Kea summit (Fig. 24) is about 6 times more than that along the coast. Compared with TER35 (Fig. 17c) with roughly the same Fr, the rainfall

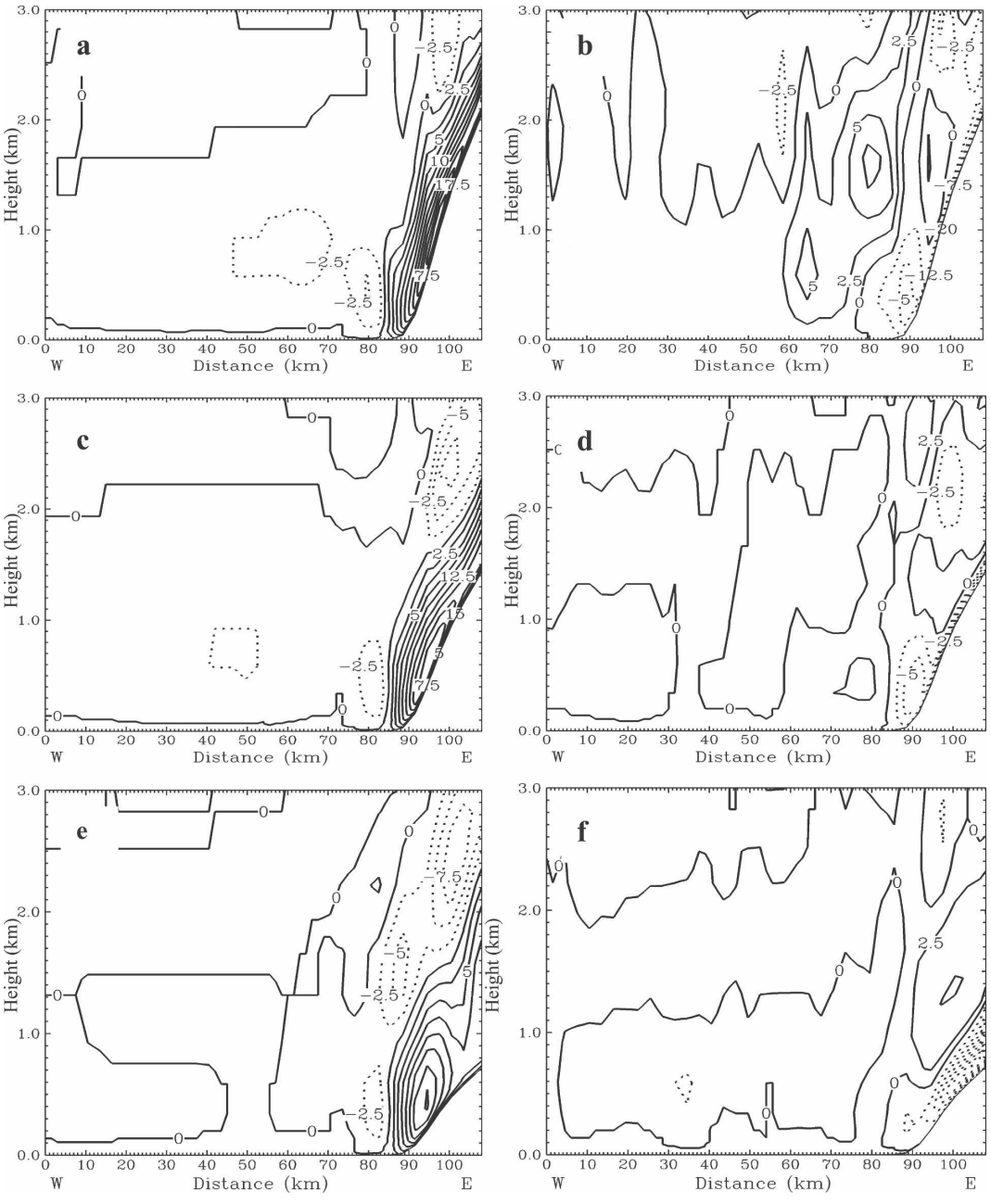

FIG. 16. Temporal mean vertical velocity (cm s^{-1}) with a contour interval of 2.5 cm s^{-1} during HaRP for the Kona transect (Fig. 8a) for the control run at (a) 1400 and (b) 0200 HST, for TER70 at (c) 1400 and (d) 0200 HST, and for TER35 at (e) 1400 and (f) 0200 HST.

maximum in S_TER is 300 mm greater and is closer to the mountaintop. It is also about 100 mm more than the rainfall maximum simulated in CTRL. Large rainfall accumulation (300 mm) also occurs close to the Mauna Loa summit. With the same mountain height, a smaller island can yield more rainfall than a larger island because of stronger orographic lifting caused by steeper slopes and less reduction of wind speed by surface friction. During the diurnal cycle, the maxima of rising motion on the windward side are 5–10 cm s^{-1} for TER35, whereas they are 15–30 cm s^{-1} for S_TER. With a stronger rising motion, the condensates are expected to stay in the air longer, to grow larger, and to be advected to upper slopes. Furthermore, from a linear theory of moist stable orographic precipitation, Smith and Barstad (2004) show that the location of maximum

TABLE 4. Some characteristics of the temporal mean katabatic/offshore flow and the dynamically induced westerly reversed flow on the lee side of the island of Hawaii at 0200 HST during the HaRP period, and the spatial mean of the rainfall accumulation (mm) for all of the grids with an elevation lower than 200 m in the quadrangle area (Fig. 1b) on the lee side of the island of Hawaii for the time period 1900–0300 HST during HaRP.

	CTRL	TER70	TER35
Fr	0.2	0.3	0.6
Max katabatic flow strength (m s^{-1})	3.5	3	—
Max extent (km) of offshore flow	18	16	—
Max depth (m) of offshore flow	400	400	—
Max rising motion (cm s^{-1})	5.2	2.6	—
Max return flow strength (m s^{-1})	2.5	1.8	0.1
Rainfall (mm)	44	13	1.2

precipitation is determined by a competition between the upstream shift caused by dynamics and the downstream shift caused by cloud delays. For a larger island, the advection time scale for the air to reach the mountaintop becomes longer (Jiang and Smith 2003); thus, the rainfall maximum tends to occur on the windward slopes. The relatively short residence times in S_TER prevent precipitation from falling over the windward slopes and hence lead to a more concentrated precipitation maximum close to mountaintops.

For Mauna Kea, the distance between the coast and the mountaintop for S_TER is about 15 km; assuming a wind speed of 6 m s^{-1}, the advection time scale is about 40 min. However, it would take the air parcel about 10 min to travel 5 km to reach the 500-m terrain height before it is lifted and reaches the level of free convection (LFC; in this case 500 m; Fig. 25). Therefore, the advection time scale between the air parcel reaching the LFC and the summit is about 30 min, which is comparable to the time scale for the development of trade wind showers (20 min) (Takahashi 1988). Thus, the maximum precipitation occurs near the mountaintop. The island of Kauai is more or less circular in shape and the advection time scale is almost independent of wind direction. Therefore, maximum rainfall tends to occur near the summit for most cases, except for high wind cases when maximum rainfall may spill over the lee side. For Mauna Loa, the advection time scale for the condensates to reach the mountaintop for the S_STER case is about 50 min, which is longer than the time required for the development of trade wind rainshowers. Thus, the maximum rainfall occurs on the windward slopes.

The diurnal rainfall maximum occurs in the evening. The 4-h rainfall accumulation maximum between 1900 and 2300 HST near Mauna Kea (Fig. 26b) is 50–100 mm more than at any other period. Near the summit of

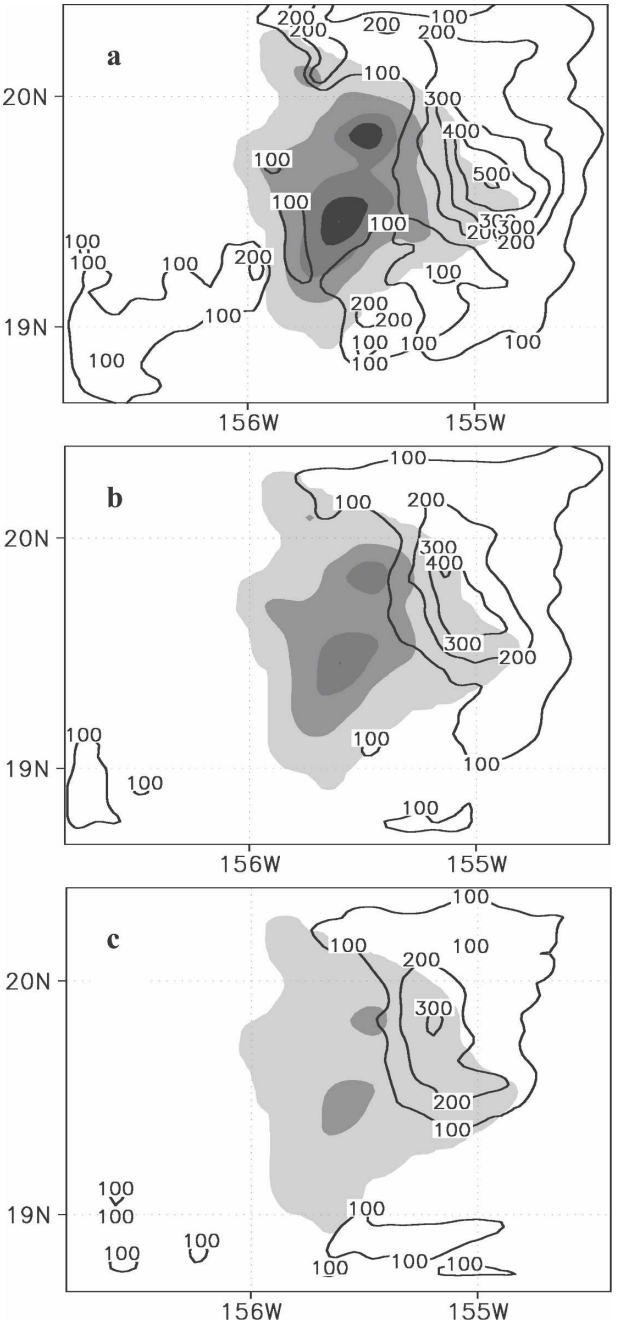

FIG. 17. The total rainfall (mm) with a contour interval of 100 mm during the HaRP period for (a) CTRL, (b) TER70, and (c) TER35.

Mauna Loa, it is 10–50 mm more than at other periods. The 4-h rainfall accumulation in the early morning (Figs. 26c and 26d) is smaller than in the evening because of weaker rising motion (Fig. 23c). Furthermore, the LFC in the early morning is higher than in the evening. Minimum rainfall occurs in the early afternoon (Fig. 26f) due to the highest LFC during the di-

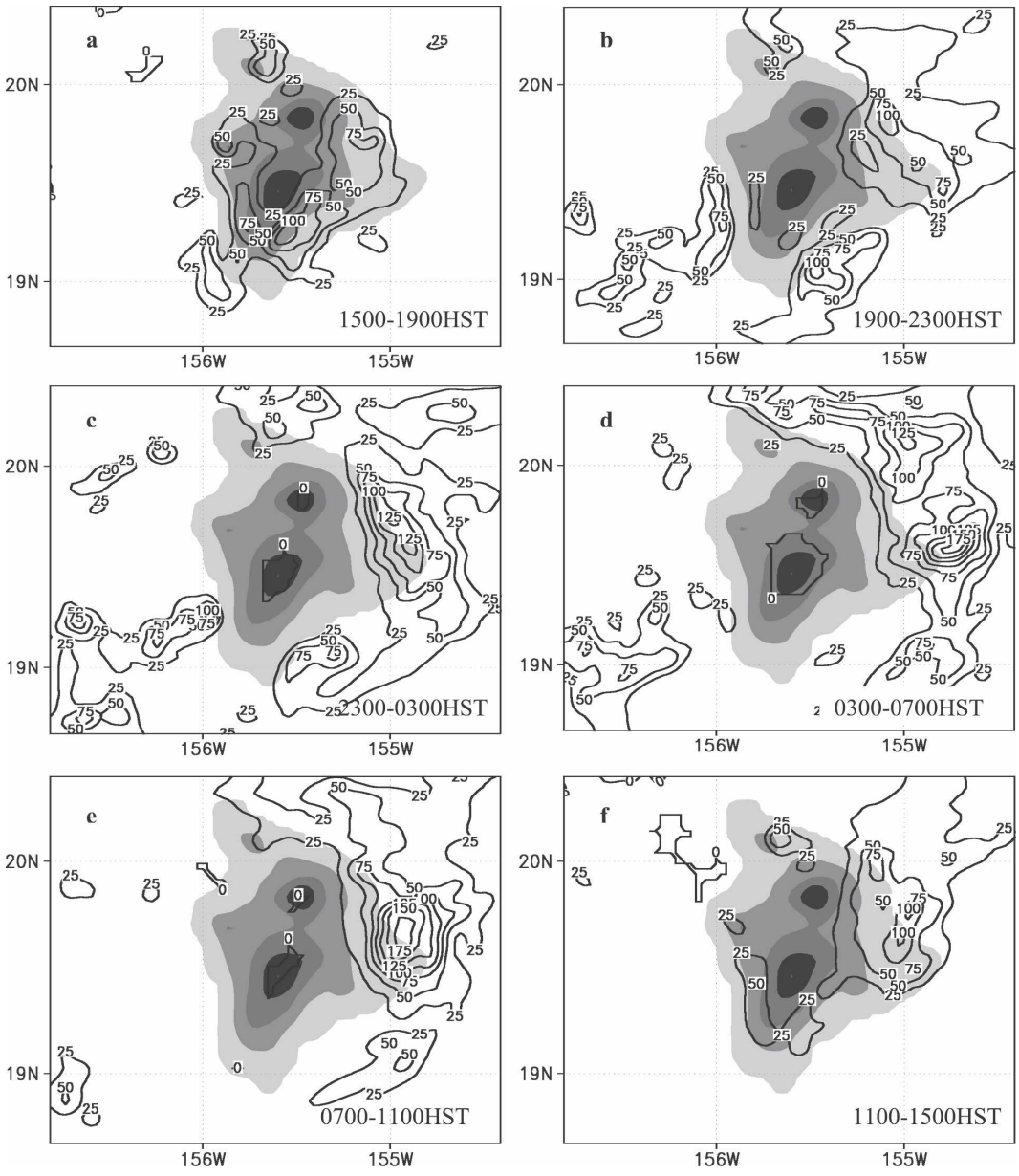

FIG. 18. The 4-h rainfall accumulation (mm) of CTRL during the HaRP period with a contour interval of 25 mm for (a) 1500–1900, (b) 1900–2300, (c) 2300–0300, (d) 0300–0700, (e) 0700–1100, and (f) 1100–1500 HST.

urnal cycle, even though the rising motion in the early afternoon (Fig. 23d) is 5–10 cm s^{-1} stronger than in the early morning (Fig. 23c).

6. Summary

In this study, we have tried to isolate two dominant factors in determining the weather and climate in Hawaii under the trade wind conditions: terrain height and island size. We use the MM5 LSM and the island of Hawaii, because the island-scale circulations and weather during the diurnal cycle for the island of Hawaii are well simulated by the model. We conducted sensitivity tests with different model terrains for the island of Hawaii to study the effects of mountain/terrain heights on island-induced circulations and rainfall throughout the diurnal cycle. We also conducted a sensitivity test with a model terrain of the island of Hawaii that was shrunk to the same height and size of the island of Kauai, to address the effects of island size on rainfall production and distribution in Hawaii.

As the model terrain becomes lower, the flow over

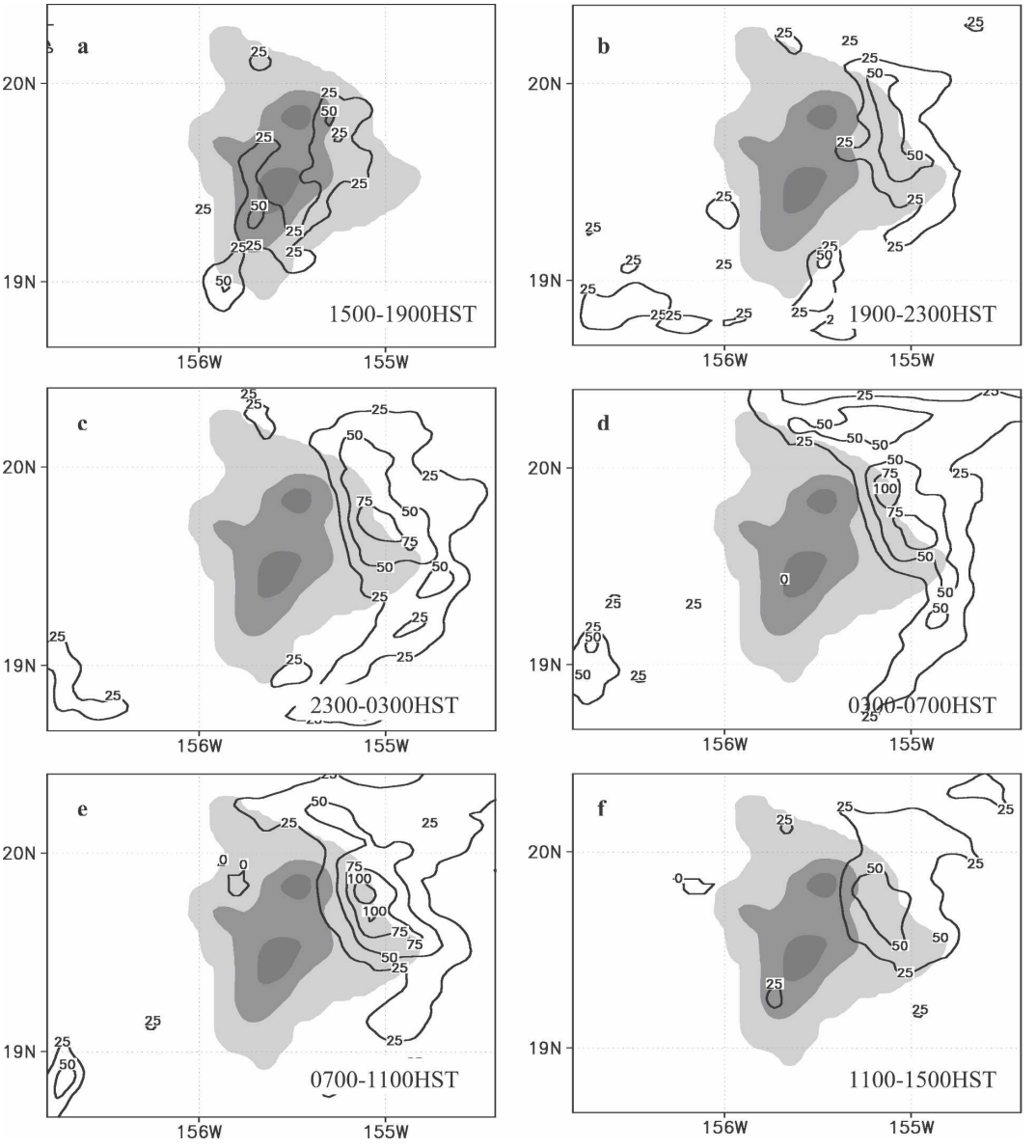

FIG. 19. As in Fig. 18 but for TER70.

the northwestern area of the island shifts to a flow regime without a return flow in the lee. To the west of the Kona coast is the large wake zone. The horizontal extent of the wake zone becomes smaller with weaker westerly return flow for a lower model terrain height. A reduction of terrain height to below the trade wind inversion allows the airflow aloft to move over the mountains with warmer air temperatures on the leeside slopes. In addition to island blocking, terrain heights also affect the land surface thermal forcing throughout the diurnal cycle. During the daytime, the land surface heating is more significant for a lower model terrain because of less cloudiness on the slope, resulting from weaker orographic lifting. At night, the land surface cooling becomes less significant for a lower model terrain as a result of reduced longwave radiation heat loss because of a thicker moist trade wind layer. During the daytime, the onshore/upslope flow on the leeside area is stronger for a lower model terrain because of stronger thermal forcing over land. On the windward side, the combined anabatic–trade wind flow in the afternoon is also stronger for a lower model terrain height because of more significant land surface heating and weaker island blocking. At night, the katabatic/offshore flow on the windward side is shallower and weaker with a smaller offshore extent for a lower terrain because of

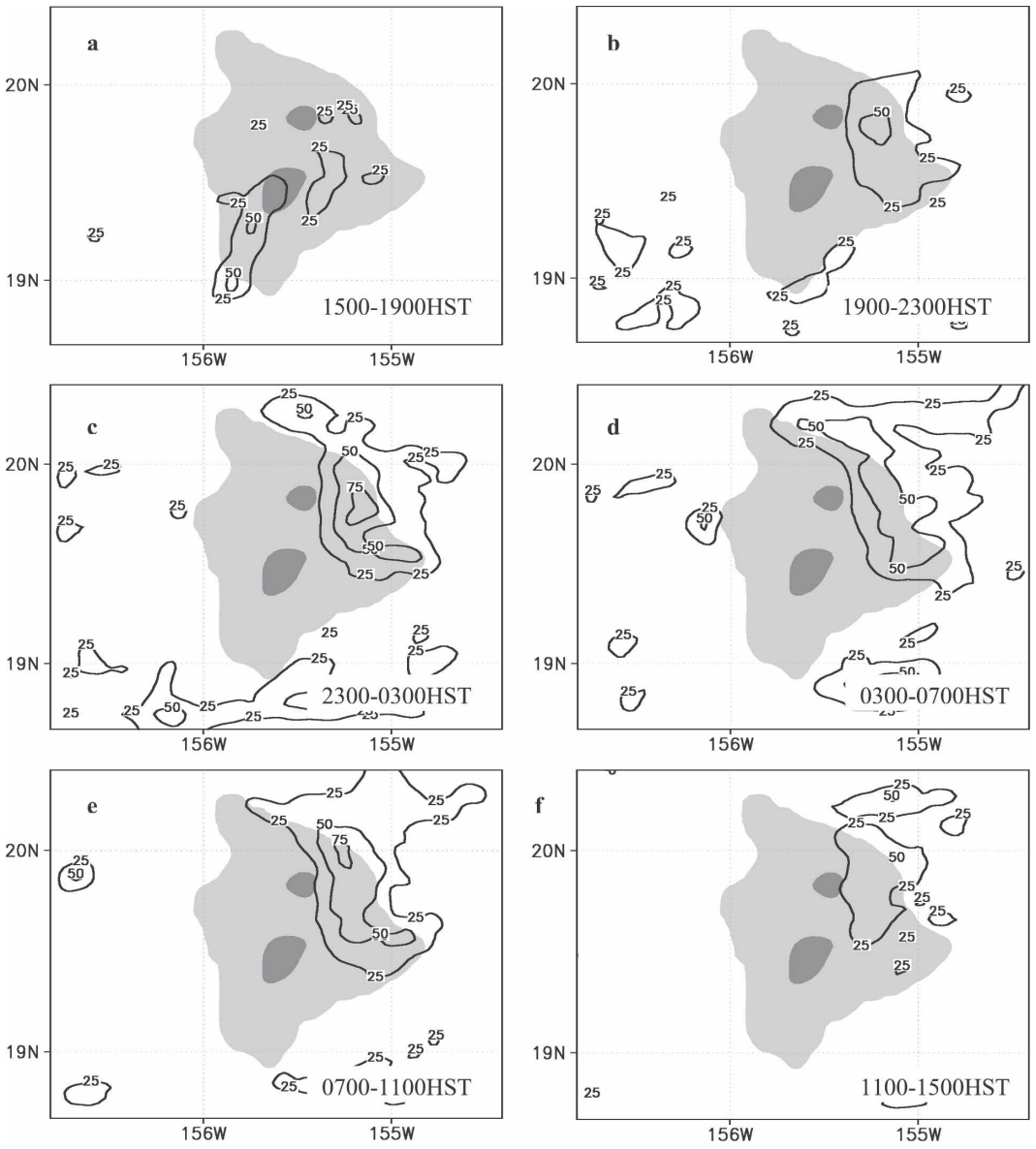

FIG. 20. As in Fig. 18 but for TER35.

a stronger incoming trade wind flow, weaker thermal forcing over land, and a less steep slope.

In addition to mountain height, island size is another factor that affects rainfall production and distribution. For a mountain height lower than the trade wind inversion, the simulated rainfall maximum is greater and closer to the mountaintop for a smaller island, because of stronger orographic lifting as a result of steeper slopes and a stronger incoming flow, and a shorter advection time scale for an air parcel to reach the mountaintop. The heavy rainfall maximum on the mountaintop of the island of Kauai is because of its suitable height and size.

Our results show that although Fr is a control parameter for flow regimes of airflow past an isolated mountain, it is not a control parameter for trade wind rainfall for either the windward or the lee sides of the island of Hawaii. From our sensitivity tests with different model terrain heights, Fr is negatively correlated with simulated rainfall. Neither dynamic forcing nor land surface forcing alone is adequate to account for the rainfall production on the windward and the lee sides. The rainfall amounts over land and the coastal regions are related to rising motions caused by nonlinear interactions among island blocking, orographic lifting, and the surface forcing.

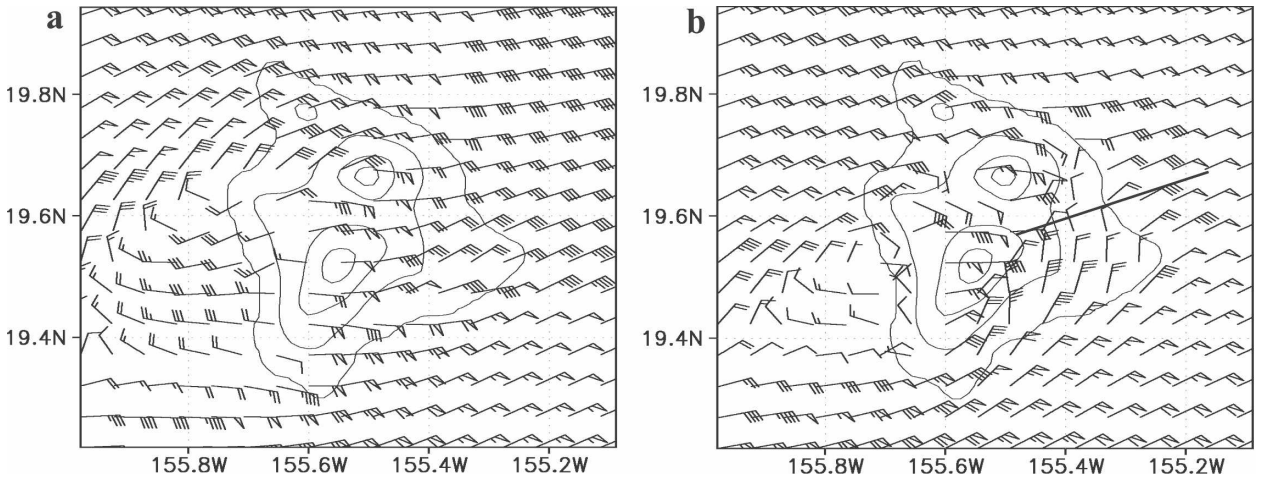

FIG. 21. Temporal mean surface winds of S_TER during the HaRP period at (a) 1400 and (b) 0200 HST with a terrain contour interval of 400 m (solid lines).

This study confirms that the evening rainfall maximum along the Kona leeward coast during the diurnal cycle is caused by the convergence between the westerly return flow and the offshore flow. For a lower model terrain, the westerly return flow is weaker and, as a result, the rainfall amounts are smaller. The nocturnal rainfall maximum on the lower windward slopes is a result of low-level convergence between katabatic flow and the incoming decelerating trade wind flow, and enhanced by orographic lifting aloft. For a lower

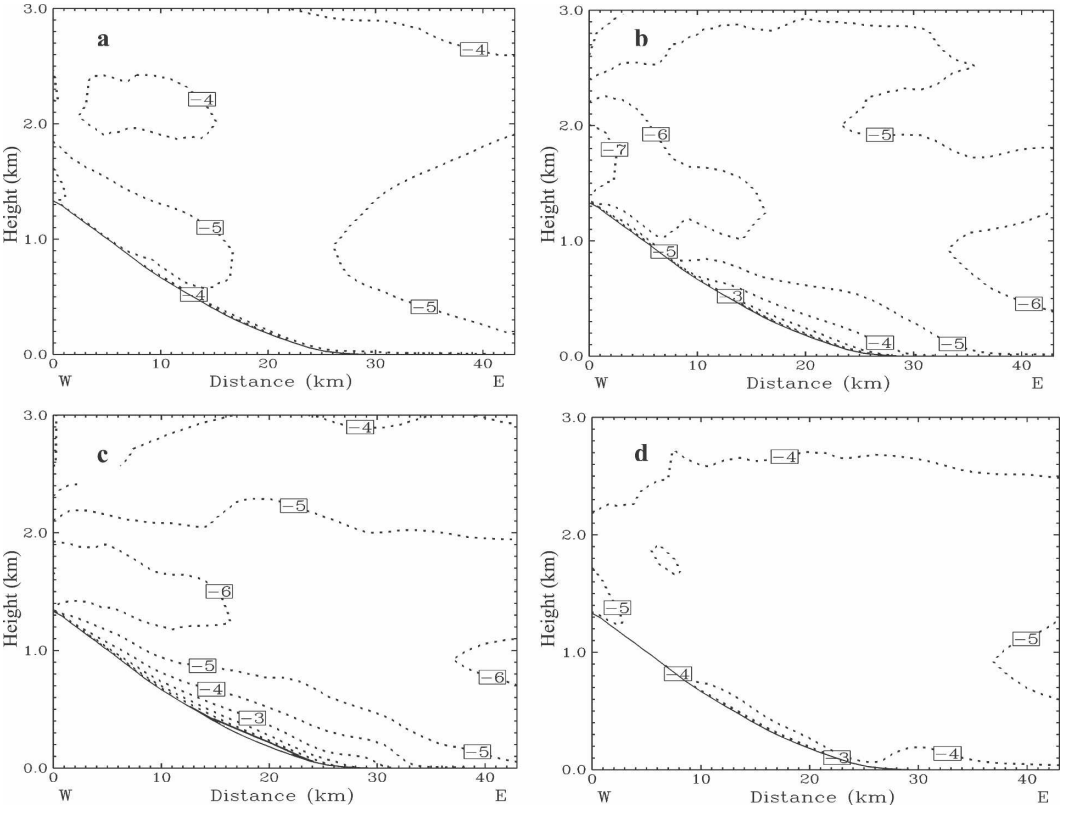

FIG. 22. Height–distance (km) cross sections for the temporal mean zonal wind speed during the HaRP period with a contour interval of 1 m s^{-1} along the transect in Fig. 21b at (a) 1700, (b) 2100, (c) 0500, and (d) 1300 HST.

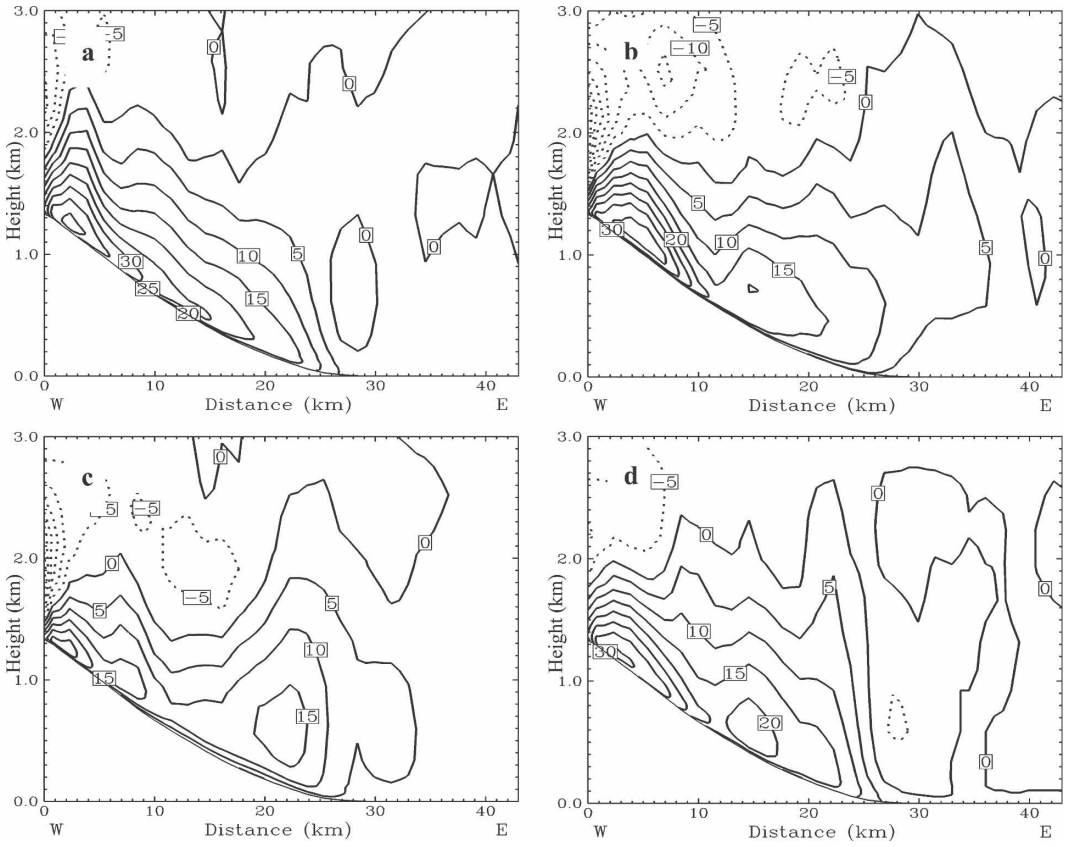

FIG. 23. Same as in Fig. 22 but for the vertical velocity with a contour interval of 5 cm s^{-1}.

model terrain, the katabatic flow is shallower and upstream flow deceleration is less significant; the nocturnal rainfall amounts are lower because of weaker rising motions. This study suggests that the rainfall amounts on the windward and leeside slopes during the day are

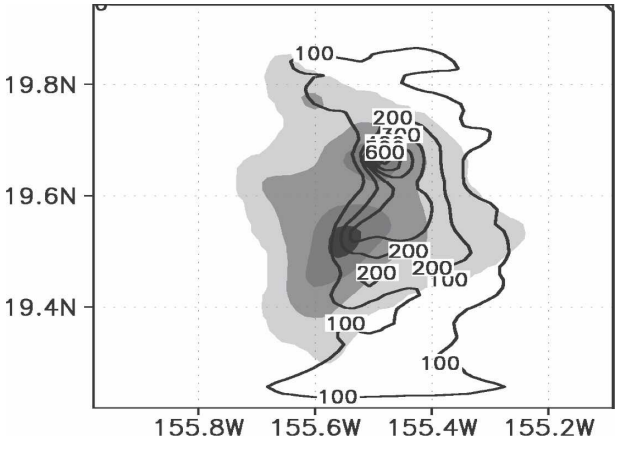

FIG. 24. The total rainfall accumulation (mm) during the HaRP period for S_TER with a contour interval of 100 mm (thick solid lines) and a terrain with gray shading scale of 400 m.

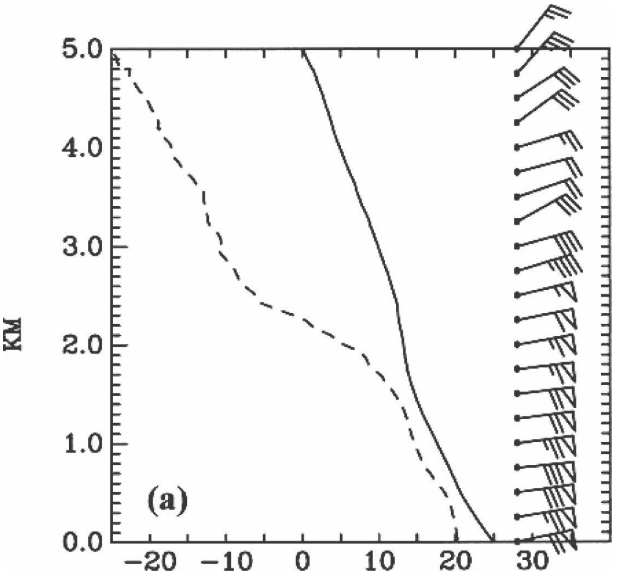

FIG. 25. The averaged sounding during HaRP based on the 20 aircraft upstream soundings, after Chen and Feng (2001): temperature (°C; solid); dewpoint (°C; dashed). The mean LFC is around 500 m.

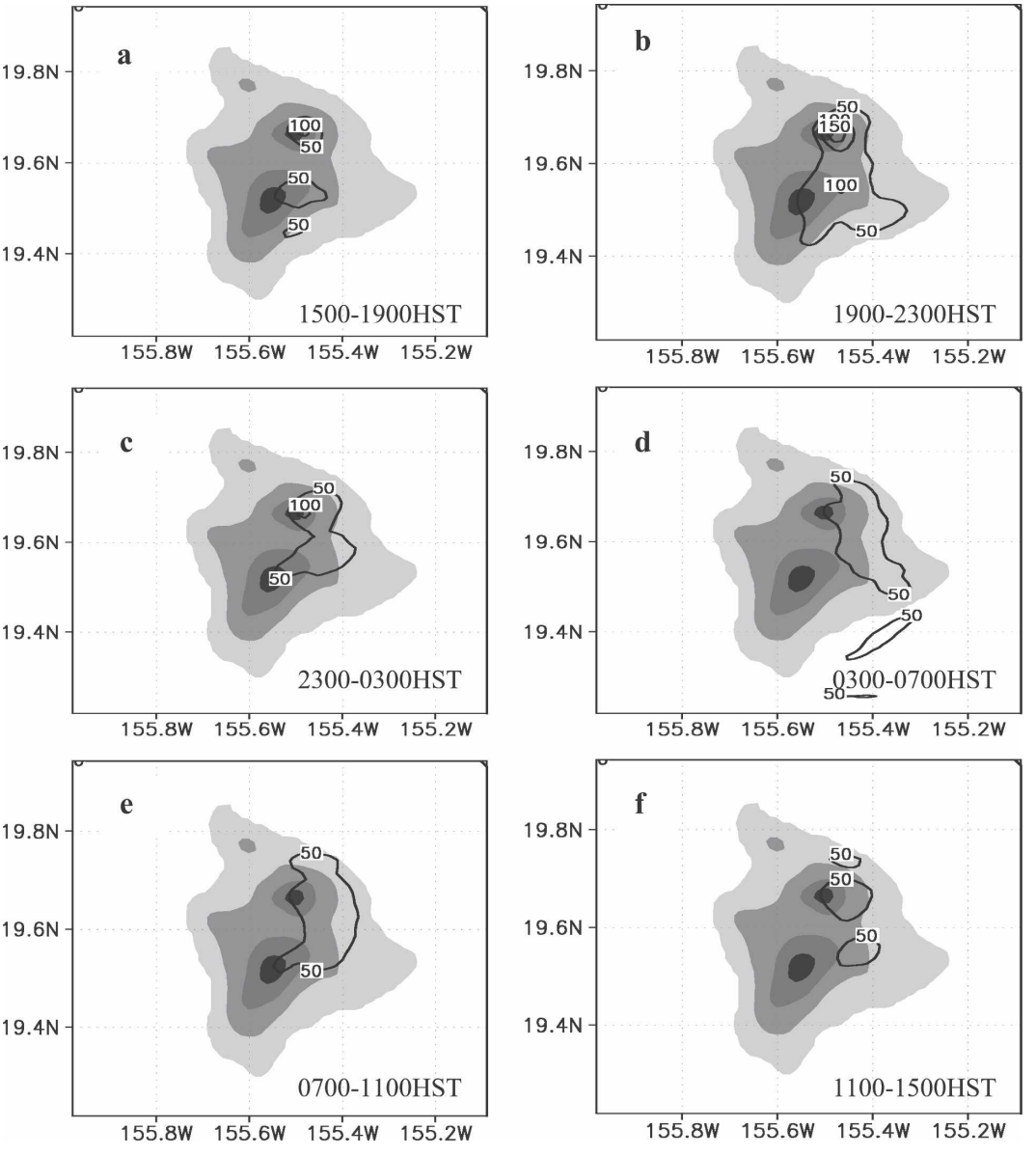

FIG. 26. The 4-h rainfall accumulation (mm) during HaRP for S_TER with a contour interval of 50 mm for (a) 1500–1900, (b) 1900–2300, (c) 2300–0300, (d) 0300–0700, (e) 0700–1100, and (f) 1100–1500 HST.

caused by orographic lifting and are smaller for a lower model terrain because of a decrease in the steepness of the mountain slope. On the windward slopes, the orographic lifting is caused by the combined trade wind–anabatic flow, whereas on the leeside slope, it is caused by the development of the anabatic flow.

Acknowledgments. The authors thank the NCAR MM5 group for the applications of the MM5 LSM model, the anonymous reviewers for their comments, and D. Henderson for editing the text. This work is supported by the National Science Foundation under Grant ATM-0140387. We thank the University of Hawaii and the Maui High Performance Computing Center (MHPCC) for their support of this project.

REFERENCES

Carbone, R. E., J. D. Tuttle, and W. C. Lee, 1995: Forcing of flow reversal along the windward slopes of Hawaii. *Mon. Wea. Rev.,* **123,** 3466–3480.

——, ——, W. A. Cooper, V. Grubišić, and W. C. Lee, 1998: Trade wind rainfall near the windward coast of Hawaii. *Mon. Wea. Rev.,* **126,** 2847–2863.

Chen, F., and J. Dudhia, 2001: Coupling an advanced land sur-

face–hydrology model with the Penn State–NCAR MM5 modeling system. Part I: Model implementation and sensitivity. *Mon. Wea. Rev.,* **129,** 569–585.

Chen, Y.-L., and A. J. Nash, 1994: Diurnal variations of surface airflow and rainfall frequencies on the island of Hawaii. *Mon. Wea. Rev.,* **122,** 34–56.

——, and J.-J. Wang, 1994: Diurnal variations of surface thermodynamic fields on the island of Hawaii. *Mon. Wea. Rev.,* **122,** 2125–2138.

——, and J. Feng, 1995: The influence of inversion height on precipitation and airflow over the island of Hawaii. *Mon. Wea. Rev.,* **123,** 1660–1676.

——, and J.-J. Wang, 1995: The effects of precipitation on the surface temperature and airflow over the island of Hawaii. *Mon. Wea. Rev.,* **123,** 681–694.

——, and J. Feng, 2001: Numerical simulations of airflow and cloud distributions over the windward side of the island of Hawaii. Part I: The effects of trade wind inversion. *Mon. Wea. Rev.,* **129,** 1117–1134.

Dudhia, J., 1993: A nonhydrostatic version of the Penn State–NCAR mesoscale model: Validation tests and simulation of an Atlantic cyclone and cold front. *Mon. Rea. Rev.,* **121,** 1493–1513.

——, and M. W. Moncrieff, 1989: A three-dimensional numerical study of an Oklahoma squall line containing right-flank supercells. *J. Atmos. Sci.,* **46,** 3363–3391.

Eber, L. E., 1957: Upper air and surface wind observation in Project Shower. *Tellus,* **9,** 558–568.

Feng, J., and Y. L. Chen, 1998: Evolution of katabatic flow on the island of Hawaii during 10 August 1990. *Mon. Wea. Rev.,* **126,** 2185–2199.

——, and ——, 2001: Numerical simulations of airflow and cloud distributions over the windward side of the island of Hawaii. Part II: Nocturnal flow regime. *Mon. Wea. Rev.,* **129,** 1135–1147.

Frye, J., and Y.-L. Chen, 2001: Evolution of downslope flow under strong opposing trade winds and frequent trade-wind rainshowers over the island of Hawaii. *Mon. Wea. Rev.,* **129,** 956–977.

Garrett, A. J., 1980: Orographic cloud over the eastern slopes of Mauna Loa volcano, Hawaii, related to insolation and wind. *Mon. Wea. Rev.,* **108,** 931–941.

Giambelluca, T. W., M. A. Nullet, and T. A. Schroeder, 1986: Rainfall atlas of Hawaii. Dept. of Land and Natural Resources Rep. R76, State of Hawaii, Honolulu, HI, 267 pp.

Grubišić, V., R. B. Smith, and C. Schär, 1995: The effect of bottom friction on shallow-water flow past an isolated obstacle. *J. Atmos. Sci.,* **52,** 1985–2005.

Hong, S.-Y., and H. L. Pan, 1996: Nonlocal boundary layer vertical diffusion in a medium-range forecast model. *Mon. Wea. Rev.,* **124,** 2322–2339.

Hsie, E.-Y., R. A. Anthes, and D. Keyser, 1984: Numerical simulation of frontogenesis in a moist atmosphere. *J. Atmos. Sci.,* **41,** 2581–2594.

Jiang, Q., and R. B. Smith, 2003: Cloud timescales and orographic precipitation. *J. Atmos. Sci.,* **60,** 1543–1559.

Lavoie, R. L., 1967: Air motions over the windward coast of the island of Hawaii. *Tellus,* **19,** 354–358.

Leopold, L. B., 1949: The interaction of trade wind and sea breeze, Hawaii. *J. Meteor.,* **8,** 533–541.

Mendonca, B. G., 1969: Local wind circulation on the slope of Mauna Loa. *J. Appl. Meteor.,* **8,** 533–541.

Nickerson, E. C., 1979: On the numerical simulation of airflow and clouds over mountainous terrain. *Beitr. Phys. Atmos.,* **52,** 161–177.

Patzert, W. C., 1969: Eddies in Hawaiian waters. HIG Rep. HIG-69-8, Hawaii Institute of Geophysics, University of Hawaii, Honolulu, HI, 51 pp.

Ramage, C. S., and T. A. Schroeder, 1999: Trade wind rainfall atop Mount Waialeale, Kauai. *Mon. Wea. Rev.,* **127,** 2217–2226.

Rasmussen, R. M., and P. K. Smolarkiewicz, 1993: On the dynamics of Hawaiian cloud bands. Part III: Local aspects. *J. Atmos. Sci.,* **50,** 1560–1572.

——, ——, and J. Warner, 1989: On the dynamics of Hawaiian cloud bands: Comparison of model results with observations and island climatology. *J. Atmos. Sci.,* **46,** 1589–1608.

Reisner, J. M., and P. K. Smolarkiewicz, 1994: Thermally forced low Froude number flow past three-dimensional obstacles. *J. Atmos. Sci.,* **51,** 117–133.

Schär, C., and R. B. Smith, 1993: Shallow-water flow past isolated topography. Part I: Vorticity production and wake formation. *J. Atmos. Sci.,* **50,** 1373–1400.

——, and D. R. Durran, 1997: Vortex formation and vortex shedding in continuously stratified flows past isolated topography. *J. Atmos. Sci.,* **54,** 534–554.

Smith, R. B., 1989: Hydrostatic flow over mountains. *Advances in Geophysics,* Vol. 31, Academic Press, 1–41.

——, and V. Grubišić, 1993: Aerial observation of Hawaii's wake. *J. Atmos. Sci.,* **50,** 3728–3750.

——, and I. Barstad, 2004: A linear theory of orographic precipitation. *J. Atmos. Sci.,* **61,** 1377–1391.

Smolarkiewicz, P. K., and R. Rotunno, 1989: Low Froude number flow past three-dimensional obstacles. Part I: Baroclinically generated lee vortices. *J. Atmos. Sci.,* **46,** 1154–1164.

——, and ——, 1990: Low Froude number flow past three-dimensional obstacles. Part II: Upwind flow reversal zone. *J. Atmos. Sci.,* **47,** 1498–1511.

——, R. M. Rasmussen, and T. L. Clark, 1988: On the dynamics of Hawaiian cloud bands: Island forcing. *J. Atmos. Sci.,* **45,** 1872–1905.

Takahashi, T., 1988: Long-lasting trade-wind rain showers in a three-dimensional model. *J. Atmos. Sci.,* **45,** 3333–3353.

Ueyoshi, K., and Y.-J. Han, 1991: A three-dimensional simulation of airflow and orographic rain over the island of Hawaii. *J. Meteor. Soc. Japan,* **69,** 127–151.

Wang, J.-J., and Y.-L. Chen, 1995: Characteristics of near-surface winds and thermal profiles on the windward slopes of the island of Hawaii. *Mon. Wea. Rev.,* **123,** 3481–3501.

Yang, Y., and Y.-L. Chen, 2003: Circulations and rainfall on the leeside of the island of Hawaii during HaRP. *Mon. Wea. Rev.,* **131,** 2525–2542.

——, ——, and F. M. Fujioka, 2005: Numerical simulations of the island-induced circulations for the island of Hawaii during HaRP. *Mon. Wea. Rev.,* **133,** 3693–3713.

Zhang, Y., Y.-L. Chen, S.-Y. Hong, K. Kodama, and H.-M. H. Juang, 2005a: Validation of the coupled NCEP Mesoscale Spectral Model and an advanced Land Surface Model over the Hawaiian Islands. Part I: Summer trade wind conditions over Oahu and a heavy rainfall event. *Wea. Forecasting,* **20,** 827–846.

——, ——, T. A. Schroeder, and K. Kodama, 2005b: Numerical simulations of the sea-breeze circulations over northwest Hawaii. *Wea. Forecasting,* **20,** 847–872.